NACA RM A54G14

NACA

RESEARCH MEMORANDUM

EFFECT OF ROTATION OF AN NACA 1-SERIES E-TYPE COWLING
ON THE INTERNAL FLOW AND FORCE CHARACTERISTICS
OF THE COWLING AT MACH NUMBERS UP TO 0.84
AND AT AN ANGLE OF ATTACK OF 0°

By Robert I. Sammonds and Robert M. Reynolds

Ames Aeronautical Laboratory
Moffett Field, Calif.

CLASSIFICATION CANCELLED

Authority _Naca Res. Abs. t_ Date _7-20-56_

_RM-104_

By _NB 8-6-56_   See _____

NATIONAL ADVISORY COMMITTEE
FOR AERONAUTICS
WASHINGTON
October 27, 1954

NATIONAL ADVISORY COMMITTEE FOR AERONAUTICS

RESEARCH MEMORANDUM

EFFECT OF ROTATION OF AN NACA 1-SERIES E-TYPE COWLING
ON THE INTERNAL FLOW AND FORCE CHARACTERISTICS
OF THE COWLING AT MACH NUMBERS UP TO 0.84
AND AT AN ANGLE OF ATTACK OF 0°

By Robert I. Sammonds and Robert M. Reynolds

SUMMARY

An investigation has been conducted to determine the effect of
rotation on the internal flow and force characteristics of an NACA
1-series E-type cowl, designed to operate with a four-blade single-
rotation propeller. Pressure recovery, internal flow angle, cowl-gap
and duct flow, thrust, and torque were measured for the cowling with-
out a propeller at Mach numbers from 0.20 to 0.84, inlet velocity ratios
from 0.19 to 0.93, and advance ratios (based on a model propeller diam-
eter of 4 feet, equivalent to a ratio of cowl diameter to propeller diam-
eter of 0.29) from 0.75 to 5.06. Included are results of surveys of the
local velocity distribution in the propeller plane. All tests were con-
ducted with the model, without a propeller, at an angle of attack of 0°
and at a Reynolds number of 1.72 million, based on the maximum diameter
of the cowl.

A ram-recovery ratio of about 0.99 was obtained at the design Mach
number of 0.80 when the cowl was operated at its design inlet velocity
ratio and rotational speed (internal blade-shank fairings operating near
zero lift). As would be expected, operation of the cowling so that the
blade-shank fairings were at positive angles of attack (any combination
of inlet velocity ratio and advance ratio, regardless of Mach number,
whose product is less than that for the design inlet velocity ratio and
advance ratio) resulted in higher recoveries than for the corresponding
zero-lift condition of operation, due to the pumping action of the blade-
shank fairings. However, this increase in recovery was accompanied by
an increase in the power required to rotate the cowl and by large changes
in the internal flow angle, up to angles greater than 40° in some con-
ditions.

Ram-recovery ratio was relatively uniform across the duct, with var-
iations of less than 4 percent at inlet velocity ratios below 0.40.

The thrust of the E-cowl was due primarily to the pressure forces
on the inner and outer surfaces of the cowl, and the pressure forces on
the spinner and the thrust forces of the blade-shank fairings were
relatively small.

INTRODUCTION

The successful application of the turbopropeller powerplant is, in part, dependent on the efficient handling of the air required by the turbine engine (ref. 1). An efficient induction system must handle large quantities of air with high recovery ratios and relatively uniform radial and circumferential distributions of flow.

Previous investigations into the efficiency of air induction systems for turbine-propeller installations have included studies of a nonrotating NACA E-type cowling (ref. 2) and several NACA D-type cowlings in combination with both single- and dual-rotation propellers (refs. 3 to 6). These investigations have been made at both low and high subsonic speeds to determine the internal flow characteristics of these types of cowls.

The purpose of the present investigation was to study the effect of cowl rotation on the internal flow characteristics and the forces on an NACA 1-series E-type cowl designed to operate with a four-blade single-rotation propeller. The tests were conducted in the Ames 12-foot pressure wind tunnel at Mach numbers up to 0.84 for various inlet velocity and advance ratios to determine the relationship of these parameters to the flow characteristics in the duct and through the cowl gap, and to the thrust and power requirements of the rotating cowl. Surveys were also made to determine the radial velocity distribution in the propeller plane.

SYMBOLS

A cross-sectional area in a plane perpendicular to the model center line

a speed of sound

C_D external drag coefficient, $\dfrac{drag}{q_oF}$

C_{D_g} cowl-gap drag coefficient, $\dfrac{m_2}{q_oF}(V_o-V_2')$

C_P power coefficient, $\dfrac{power}{\rho n^3 D^5}$

D propeller diameter
             (Thrust and power coefficients and advance ratio are based on a 4-foot diameter, equivalent to a ratio of maximum cowl diameter to propeller diameter of 0.29.)

F frontal area of cowling

H   average total pressure

$\dfrac{H - p_0}{H_0 - p_0}$ ram-recovery ratio

J   advance ratio, $\dfrac{V}{nD}$

M   Mach number, $\dfrac{V}{a}$

m   mass rate of flow, ρAV

n   rotational speed

P   pressure coefficient, $\dfrac{p - p_0}{q_0}$

p   static pressure

q   dynamic pressure, $\dfrac{\rho V^2}{2}$

r   radius from center of rotation

T_c thrust coefficient, $\dfrac{\text{thrust}}{\rho V^2 D^2}$

U   local velocity in propeller plane

V   air-stream velocity

$V_2{}'$ calculated cowl-gap velocity, assuming expansion to p_0

$\dfrac{V_1}{V_0}$ inlet velocity ratio

W_a weight rate of flow, $g\rho AV$

β   angle of the chord of the blade-shank fairing with respect to
              the propeller plane of rotation

θ   internal flow angle, the angle of the resultant of the axial
              and tangential velocity components of the flow in the duct
              with respect to the axial component of the flow

ρ   mass density of air

Subscripts

The numerical subscripts refer to stations shown in figure 1.

0   free stream

1   cowling inlet

2   cowl-gap exit

3   ram-recovery rake location

MODEL

The E-type cowling which was investigated was designed to rotate with a four-blade single-rotation propeller and consisted of an NACA 1-51-117 external cowl and an NACA 1-41.43-042.86 internal spinner interconnected by four propeller-blade-shank fairings having NACA 0030-34.5 sections. A sketch of the general model arrangement showing the principal model dimensions, the geometry of the gap between the rotating and stationary portions of the cowl, and the variation of duct area with longitudinal station is presented in figure 1. Coordinates for the internal and external contours of the model are listed in table I. The design information for the model is given in reference 2. A photograph of the model mounted on the 1000-horsepower dynamometer in the Ames 12-foot pressure wind tunnel is shown in figure 2.

The model, back to 16.38 inches behind the leading edge of the cowl, was identical to the nonrotating E-cowl described in reference 2, except for the addition of twist to the blade-shank fairings and for a small difference in the cowl-gap dimensions. (Gap area of the nonrotating cowl was about 10 percent larger than the gap area of the rotating cowl due to difficulties encountered in assembling the nonrotating model.) The gap for the rotating cowl was designed to provide for a leakage air flow through the gap equal to 17 percent of the flow through the inlet at the design condition. The twist of the NACA 0030-34.5 blade-shank fairings, listed in table II and shown in figure 3, was such as to provide approximately zero lift (assuming the flow at the blade-shank fairings was in the axial direction and that the velocity was uniform across the duct) at the design conditions of a Mach number of 0.80, an advance ratio of 3.7, and an inlet velocity ratio of 0.3.

The instrumentation of the model consisted of total- and static-pressure tubes in the cowl gap (station 2, fig. 1), and total-pressure, static-pressure, and yaw rakes in the duct (station 3, fig. 1).

The six total- and six static-pressure tubes in the cowl gap were
spaced alternately 30° apart, at a measuring station 9.85 inches behind
the leading edge of the cowl. The four shielded total-pressure rakes at
station 3 are shown in figure 3. Each consisted of nine tubes disposed
radially across the duct in such a manner that each tube was in the center
of an area equal to one-thirty-sixth of the total duct area. Calibration
of the total-pressure rakes indicated that the rakes were accurate within
1 percent of the impact pressure at angles of attack up to 40° for Mach
numbers up to 0.85. The two static-pressure rakes at station 3 each con-
sisted of nine tubes disposed radially across the duct, with the tubes
being located at the same radial stations used for the total-pressure rake.
No attempt was made to calibrate the static rakes as they were considered
to have the accuracy required for the calculation of the inlet velocity
ratio.

The yaw rake at station 3 consisted of five yaw heads (fig. 4) dis-
posed radially across the duct in such a manner that each yaw head was in
the center of one of five concentric rings of equal area.

The static-pressure rake used to survey the air stream in the propel-
ler plane consisted of 24 static-pressure tubes at the radii listed in
table III.

TESTS AND REDUCTION OF DATA

In the investigation reported herein, measurements were made of the
pressure recoveries and flow angles in the duct, of the flow through the
duct and the cowl gap, and of the thrust and torque of the rotating cowl
operating without a propeller. Tests were conducted through the range of
Mach numbers, inlet velocity ratios, and rotational speeds tabulated below:

Mach number, M_O	Inlet velocity ratio, V_1/V_O	Advance ratio, V_O/nD
0.20	0.20 to 0.93	0.75 to 3.01
.30	.23 to .88	1.12 to 3.04
.40	.24 to .86	1.50 to 4.00
.60	.21 to .82	2.21 to 4.98
.70	.19 to .78	2.63 to 4.95
.80	.21 to .74	2.97 to 5.00
.84	.20 to .72	3.08 to 5.06

Measurements of the local velocities in the propeller plane were made with the cowl at a constant rotational speed (2,000 rpm) and for inlet velocity ratios ranging from 0.19 to 0.94 and for Mach numbers from 0.20 to 0.84.

All tests were conducted with the model, without a propeller, at an angle of attack of $0°$ and at a Reynolds number of 1.72 million, based on the maximum diameter of the cowl.

The free-stream Mach number used in this report was taken as the average Mach number over the disc area within a 4-foot diameter, as determined by velocity surveys reported in reference 7. The Mach number was corrected for the wind-tunnel blockage due to the cowl by the method of reference 8, but in no case did this correction exceed 1 percent.

The advance ratio was calculated using a diameter of 4 feet in order to permit comparison of the force data with those in reference 9.

The inlet velocity ratio, calculated in accordance with the method of reference 10, can be readily converted to mass-flow ratio by use of figure 4 of reference 10.

In the cases where ram-recovery ratio is presented as a function of radial location in the duct, the ram-recovery ratio at any radius is the arithmetic average of the recoveries at the four total-pressure tubes at that radius. All other values of ram-recovery ratio were computed from an arithmetic average of the readings from all 36 total-pressure tubes, which is equivalent to an area-weighted average.

The drag coefficient due to the momentum loss in the air flow through the cowl gap was computed assuming that the flow in the gap discharged to free-stream static pressure. In other words, the exit velocity (V_2') was computed using free-stream static pressure (p_0) and local total pressure (H_2).

The flow angle in the duct was computed from the differential pressure across the yaw head, using a calibration relating the differential pressure to the angle of flow. However, in order to know the true angle of flow in the duct, the yaw head in the duct must have the same alinement with the undisturbed air stream as it had for the calibration. Due to the difficulty of alining the yaw heads with the axis of rotation, it was found that at the design condition of inlet velocity ratio and advance ratio, the individual yaw heads indicated flow angles which varied in a random manner across the duct and had values ranging from $0°$ to $5°$ with an average value of $2°$. In order to provide a base value from which to measure flow angles at the various radial stations, it was assumed that the flow angles were $0°$ at the design condition of near zero lift on the blade-shank fairings. The angles presented throughout the report are thus the difference between the indicated angle at any given condition

and the indicated angle for the design condition. The angle was considered to be positive when the direction of the flow rotation and the cowl rotation were the same. The cowl rotation was counterclockwise when viewed looking downstream.

A calibration of the yaw rake was made for angles of yaw from $-20°$ to $+20°$ at Mach numbers up to 0.84. During tests of the rotating cowl at combinations of low inlet velocity ratios and low advance ratios at low Mach numbers, angles in excess of the calibration limits were indicated, making necessary an extrapolation of the results of the calibration to angles in excess of $40°$. The calibration curves for a similar type of yaw head (ref. 11) show that a linear extrapolation of the calibration data to an angle of $40°$ resulted in indicated angles that were high by about 10 percent. Granted the initial assumption of zero flow angle for the design condition, the accuracy of measurement of the flow angles is considered to be within $±1°$ for flow angles between $±20°$. For flow angles in excess of $20°$, the angles measured are probably high by approximately 10 percent.

The thrust, torque, and rotational speed of the cowl were measured on a dynamometer in a manner similar to that reported in reference 7. As presented herein, the thrust is the resultant longitudinal force produced by the spinner-cowling combination with the average static pressure in the duct (station 3) as the pressure assumed to be acting on the maximum cross-sectional area of the spinner. These pressures are shown in coefficient form in figure 5 as a function of inlet velocity ratio. It may be noted that propeller-shaft tension may be obtained by subtracting from the thrust values the product of these static pressures and the cross-sectional area of the propeller shaft.

The analysis of the accuracy of the thrust measurements, presented in reference 7, indicated that the error in the indicated thrust was, for the most part, less than 1 percent of the applied load. The torque of the rotating cowl, however, was less than 2.5 percent of the capacity of the torquemeter and the measured torque is not considered to be as accurate as the data presented in reference 7.

The local velocities in the propeller plane were calculated using the measured local static pressure and free-stream total pressure and were corrected for the rake calibration and for the radial velocity gradient in the tunnel (ref. 7) due to the influence of the dynamometer body.

RESULTS

The ram-recovery ratios obtained at station 3 for various Mach numbers, inlet velocity ratios, and advance ratios are presented in figure 6

as a function of advance ratio, in figure 7 as a function of inlet
velocity ratio, and in figure 8 as a function of radial station. Ram-
recovery ratios for the nonrotating E-type cowl (ref. 2) and an NACA
D-type cowl (ref. 3) are included in figure 7 for comparison.

The total and static pressures in the gap (station 2) between the
rotating and stationary portions of the cowling are presented in figure 9
as ratios (gap to duct total pressures) and pressure coefficients for
selected Mach numbers and advance ratios. The drag coefficient due to
the momentum loss in the air flow through the cowl gap for the rotating
cowl is compared in figure 10 with similar results calculated for the non-
rotating cowl and with the external drag of the nonrotating cowl (from
ref. 2). The ratio of the weight rate of flow through the cowl gap to
the weight rate of flow at the inlet for the rotating cowl is compared
in figure 11 with similar results (from ref. 2) for the stationary cowl.

The internal flow angles at station 3 for various Mach numbers,
inlet velocity ratios, and advance ratios are presented in figure 12 as
a function of advance ratio, in figure 13 as a function of inlet velocity
ratio, and in figure 14 as a function of radial station.

The thrust and power coefficients for the rotating cowl are pre-
sented in figure 15 for selected Mach numbers and advance ratios.

The distribution of velocity in the propeller plane is listed in
table III and is presented in figure 16 for a few typical Mach numbers
and inlet velocity ratios.

DISCUSSION

Internal-Flow Characteristics

Ram recovery.- It can be shown, with reference to the velocity dia-
gram given in figure 17, that a change in either the advance ratio or
the inlet velocity ratio will result in a change in the angle of attack
at which the blade-shank fairing is operating, and it can be seen from
figure 15(d) that an increase in the angle of attack of the blade-shank
fairings is accompanied by an increase in the power required to rotate
the cowl. With the blade sections operating in the duct, as is the case
with an E-cowl, any change in thrust due to a change in angle of attack
and power will be accompanied by a change in pressure recovery. This can
readily be seen in figure 6 where the data show that either decreasing
inlet velocity ratio, for a constant advance ratio, or decreasing advance
ratio, for a constant inlet velocity ratio, generally resulted in an
increase in the recoveries at station 3 as a result of the pumping action
of the blade-shank fairings. However, operation of the blade-shank fair-
ings at negative angles of attack (a combination of high inlet velocity

ratio and high advance ratio) or in a stalled condition at high positive
angle of attack (a combination of low inlet velocity ratio and low advance
ratio) would be expected to result in large losses in recovery. The
losses in pressure recovery at negative angles of attack are due to the
blade-shank fairing operating as a turbine and absorbing energy from the
air stream. This effect is also readily apparent in figure 6.

The effect of rotation on the recoveries at station 3 is shown in
figure 7, where the recoveries for both the rotating and stationary
E-cowls are compared. At the design condition ($M = 0.8$, $V_1/V_0 = 0.3$,
$J = 3.7$) for which the blade-shank fairings were designed to operate at
approximately $0°$ angle of attack, the recoveries for the two configura-
tions were in good agreement. At any other zero-lift condition, where
the product of inlet velocity ratio and advance ratio equaled the product
of the design inlet velocity ratio and advance ratio ($V_1/nD = 1.11$, see
fig. 17), the recovery for the rotating E-cowl was also in good agreement,
regardless of Mach number, with that for the stationary model. For the
reasons explained previously with regard to figure 6, operation of the
blade-shank fairings at positive angles of attack ($V_1/nD < 1.11$) resulted
in higher recoveries for the rotating cowl; conversely, operation of the
blade-shank fairings at negative angles of attack ($V_1/nD > 1.11$) resulted
in lower recoveries than those for the stationary cowl.

A comparison of the recoveries obtained with the rotating E-cowl and
those obtained with the D-cowl of reference 3 shows that, at the respec-
tive design conditions ($M = 0.8$, $J = 3.7$, $V_1/V_0 = 0.30$ for the E-cowl;
$M = 0.8$, $J = 3.7$, $V_1/V_0 = 0.42$ for the D-cowl), the E-cowl recoveries were
higher by about 13 percent (fig. 7). It should be noted in comparing the
recoveries for the E- and D-type cowls that the design inlet velocity
ratio for the D-type cowl was somewhat below the optimum value. (Optimum
inlet velocity ratio is at the knee of the recovery curve of figure 7.)
If, on the basis of the data in reference 3, the D-type cowl-spinner com-
bination had been redesigned so that it operated at a more favorable
inlet velocity ratio, the difference in performance of the two types of
cowls would probably have been decreased. It can also be seen from
figure 7 that the effect of inlet velocity ratio on the pressure recov-
eries was reversed for the two types of cowls. It may be noted that the
D-cowl tests were made with an operating propeller, whereas the E-cowl
tests were made without a propeller. However, the addition of a propel-
ler is not expected to result in any large changes in the internal flow
characteristics of the E-cowl.

As shown in both figures 6 and 7, average ram-recovery ratios in
excess of 90 percent were obtained throughout the range of the tests,
with a recovery of 99 percent being obtained at the design condition.

The pressure recovery (fig. 8) was relatively uniform across the
duct. Variations of less than 4 percent occurred at inlet velocity
ratios below 0.4. At inlet velocity ratios above 0.4, the recoveries

remained relatively uniform over the midportion of the duct but decreased quite rapidly at both the inner and outer surfaces. The static pressures measured in the duct at station 3 were also nearly uniform across the duct for all of the test conditions.

Cowl-gap flow.- Comparison of the data on cowl-gap flow for the rotating and stationary E-cowl models shows that generally greater losses occurred in the gap of the rotating cowl (fig. 9(c)) as a result of the combined effects of the smaller gap dimensions and the rotation of the cowl. It can also be seen from figure 9(c) that the effect of Mach number on the ratio of the total pressure in the gap to the total pressure in the duct was more pronounced for the rotating cowl. Losses in total-pressure ratio up to 30 percent occurred at high inlet velocity ratios and high Mach numbers. Pressure coefficients in the cowl gap (fig. 9(d)) were slightly lower for the rotating cowl than for the stationary cowl, but the effect of inlet velocity ratio on the pressure coefficients was about the same for both cowls. The effect of rotation on the total-pressure ratio (fig. 9(a)) and pressure coefficient (fig. 9(b)) for the flow in the cowl gap was relatively small at the low Mach numbers but became much larger at high Mach numbers and low inlet velocity ratios.

In order to analyze further the effect of rotation on the losses in the cowl gap, calculations were made of the drag due to the momentum loss in the air flow through the cowl gap for the rotating cowl and for the nonrotating cowl of reference 2. These data are compared in figure 10 and show that the momentum losses in the gap of the rotating cowl were higher than those for the nonrotating cowl. At the design condition of operation, the cowl-gap drag coefficient increased from 0.001 to 0.005. It can also be seen from figure 10 that the effect of compressibility on the cowl-gap drag coefficient was negligible for the stationary model; whereas the drag coefficient for the rotating model increased slightly with increasing Mach number.

Figure 10 also shows a comparison of the cowl-gap drag coefficients for the rotating and stationary models with the external drag of the non-rotating cowl (from ref. 2). For the nonrotating model, the momentum drag of the cowl-gap air flow was approximately 5 percent of the external drag of the cowl at the design condition. Similar comparison cannot be made for the rotating cowl, since the effect of rotation on the external drag of the cowl is not known.

As shown in figure 11, the variation, with inlet velocity ratio, of the ratio of the weight rate of flow through the cowl gap to the weight rate of flow through the cowl inlet for the rotating cowl was similar to that shown in reference 2 for the nonrotating cowl. However, the weight flow ratio for the rotating model was smaller over the entire range of inlet velocity ratios at which the model was tested, as a result of the smaller gap area (by about 10 percent) used for the rotating model, and the increased pressure losses in the gap. At the design condition

($M = 0.8$, $V_1/V_0 = 0.3$, $J = 3.7$) the weight flow ratio for the rotating
model was about 0.12, which is considerably lower than either the design
weight flow ratio (0.17) or that for the stationary model (0.19, ref. 2).

Internal flow angles.- In order to define more fully the flow in the
duct behind the E-cowl, measurements were made at station 3 to determine
the flow angles caused by the rotation of the cowl. These measurements
show (figs. 12 to 14) that the flow angle at station 3 was a function of
inlet velocity ratio and rotational speed as a result of the change in
the angle of attack of the propeller-blade-shank fairings, and that an
increase in the angle of attack (decrease in inlet velocity and advance
ratio) resulted in an increase in the flow angle. Further study of
figure 12 shows that the largest flow angles occurred near the outer sur-
face of the duct where, at the extreme condition of low inlet velocity
ratio and high rotational speed, angles in excess of 40° were measured.
As previously discussed in the section "Test and Reduction of Data," the
internal flow angle for the design condition ($M = 0.8$, $V_1/V_0 = 0.3$,
$J = 3.7$) was assumed to be zero (fig. 13). On the basis of this assump-
tion, figure 13 shows that for any condition when the product of inlet
velocity ratio and advance ratio was equal to the product of the design
inlet velocity ratio and advance ratio ($V_1/nD = 1.11$), the flow angle
was zero regardless of Mach number. Figure 13 also shows that for a
given radial station and advance ratio, the effect of Mach number on the
variation of the internal flow angle with inlet velocity ratio was neg-
ligible. For a given inlet velocity ratio, the variation of the internal
flow angle with radial station was small, generally less than 5°, as
shown in figure 14.

Force Characteristics

The thrust of the rotating E-cowl, presented in coefficient form
in figures 15(a) and (c), consists (aside from the skin-friction forces)
of the thrust due to the pressure on the cowl and spinner surfaces, and
the thrust developed by the propeller-blade-shank fairings. It is shown
from the pressure distributions (ref. 2) over the nonrotating cowl and
spinner surfaces that, for a given Mach number, the pressure force on
the cowl was primarily a function of inlet velocity ratio. Also, as pre-
viously discussed, the thrust force developed by the propeller-blade-
shank fairings was a function of both inlet velocity ratio and advance
ratio. In order to ascertain the relative magnitude of these thrust
forces, an analysis of the pressure forces on the nonrotating cowling
was made using the pressure distributions presented in reference 2 and
the spinner-base pressure coefficients given in figure 5. Although this
analysis gave only qualitative results, the general trend and magnitude
of the data indicated that the predominant portion of the total thrust
of the E-cowl was due to the pressure on the inner and outer surfaces of

the cowl, and that the pressure forces on the spinner and the thrust
forces of the blade-shank fairings were relatively small.

The power coefficients measured for the rotating cowl (figs. 15(b)
and (d)) were small in comparison to those obtained for the model propel-
ler of reference 9, but have been presented to show that the expected
trend of increasing power coefficient with either increasing rotational
speed or decreasing inlet velocity ratio was substantiated.

<div align="center">Velocity Distributions</div>

Velocity distributions were measured in the propeller plane in order
to obtain data useful in the design of propellers for use with NACA
E-type cowls. These data, presented in table III and figure 16, show
that velocities considerably in excess of free-stream velocity occurred
near the outer surface of the cowl. At the design condition (M = 0.8,
$V_1/V_0 = 0.3$, J = 3.7) the velocity at the surface of the cowl exceeded
the free-stream velocity by about 13 percent. The effect of inlet veloc-
ity ratio on the local velocity ratio was small for the test range of
Mach numbers and inlet velocity ratios.

<div align="center">CONCLUDING REMARKS</div>

The following summarizing remarks may be made regarding the results
of the subject investigation:

Operation of the rotating cowl at advance ratios and inlet velocity
ratios whose product equaled that for the design inlet velocity ratio
and advance ratio (blade-shank fairings at near zero lift condition)
resulted in ram-recovery ratios of 0.98 or better. At any condition of
operation (regardless of Mach number) where the product of inlet velocity
ratio and advance ratio was less than that for the design condition, the
ram-recovery ratio was greater than that for the corresponding zero lift
condition, due to the pumping action of the blade-shank fairings. However,
this increase in recovery was accompanied by an increase in the power
required to rotate the cowl and by large changes in the internal flow
angles, up to angles greater than 40° in some conditions. Conversely,
operation of the cowl at inlet velocity ratios and advance ratios whose
product was greater than that for the design condition resulted in lower
recoveries, negative flow angles, and decreased power coefficients due
to the blade-shank fairings operating as a turbine and absorbing energy
from the internal flow.

Ram-recovery ratio was relatively uniform across the duct with vari-
ations of less than 4 percent at inlet velocity ratios below 0.40.

The ratio of the weight rate of flow through the cowl gap to the weight rate of flow through the cowl inlet increased with decreasing inlet velocity ratio but was practically unaffected by rotational speed and only slightly affected by Mach number. For the design condition, the weight flow ratio was 0.12 as compared to the design value of 0.17.

The thrust of the E-cowl was due primarily to the pressure on the inner and outer surfaces of the cowl, and the pressure forces on the spinner and the thrust forces of the blade-shank fairings were relatively small.

For the design condition, the local velocity in the propeller plane exceeded the free-stream velocity by as much as 13 percent near the outer surface of the cowl. The local velocity ratios, however, were not greatly affected by either inlet velocity ratio or Mach number.

Ames Aeronautical Laboratory
        National Advisory Committee for Aeronautics
              Moffett Field, Calif., July 14, 1954

REFERENCES

1. Hanson, Frederick H., Jr., and Mossman, Emmet A.: Effect of Pressure Recovery on the Performance of a Jet-Propelled Airplane. NACA TN 1695, 1948.

2. Reynolds, Robert M., and Sammonds, Robert I.: Subsonic Mach and Reynolds Number Effects on the Surface Pressures, Gap Flow, Pressure Recovery, and Drag of a Nonrotating NACA 1-Series E-Type Cowling at an Angle of Attack of 0°. NACA RM A51E03, 1951.

3. Sammonds, Robert I., and Molk, Ashley J.: Effects of Propeller-Spinner Juncture on the Pressure-Recovery Characteristics of an NACA 1-Series D-Type Cowl in Combination With a Four-Blade Single-Rotation Propeller at Mach Numbers up to 0.83 and at an Angle of Attack of 0°. NACA RM A52D01a, 1952.

4. Molk, Ashley J., and Reynolds, Robert M.: Effects of Two Spinner Shapes on the Pressure Recovery in an NACA 1-Series D-Type Cowl Behind a Three-Blade Propeller at Mach Numbers up to 0.80. NACA RM A53L29a, 1954.

5. Keith, Arvid L., Jr., Bingham, Gene J., and Rubin, Arnold J.:
    Effects of Propeller-Shank Geometry and Propeller-Spinner-
    Juncture Configuration on Characteristics of an NACA 1-Series
    Cowling-Spinner Combination With an Eight-Blade Dual-Rotation
    Propeller. NACA RM L51F26, 1951.

6. Bingham, Gene J., and Keith, Arvid L., Jr.: Effects of Compressi-
    bility at Mach Numbers up to 0.8 on Internal-Flow Characteristics
    of a Cowling-Spinner Combination Equipped With an Eight-Blade Dual-
    Rotation Propeller. NACA RM L53E12, 1953.

7. Reynolds, Robert M., Buell, Donald A., and Walker, John H.: Investi-
    gation of an NACA 4-(5)(05)-041 Four-Blade Propeller With Several
    Spinners at Mach Numbers up to 0.90. NACA RM A52I19a, 1952.

8. Herriot, John G.: Blockage Corrections for Three-Dimensional-Flow
    Closed-Throat Wind Tunnels, With Consideration of the Effect of
    Compressibility. NACA Rep. 995, 1950. (Supersedes NACA RM A7B28)

9. Reynolds, Robert M., Sammonds, Robert I., and Kenyon, George C.:
    An Investigation of a Four-Blade Single-Rotation Propeller in Com-
    bination With an NACA 1-Series D-Type Cowling at Mach Numbers up
    to 0.83. NACA RM A53B06, 1953.

10. Smith, Norman F.: Numerical Evaluation of Mass-Flow Coefficient
    and Associated Parameters from Wake Survey Equations. NACA
    TN 1381, 1947.

11. Reid, Elliott G.: Wake Studies of Eight Model Propellers. NACA
    TN 1040, 1946.

TABLE I.- COWLING-SPINNER COORDINATES
[Coordinates in inches]

Distance from leading edge of cowl (x)	NACA 1-51-117 cowl, radius (r_c)	Outer duct, radius (r_i)	NACA 1-41.43-042.86 spinner, radius (r_s)
0	3.654	3.654	- - -
.25	4.083	3.530	- - -
.50	4.271	3.514	0
.75	4.429	3.571	.633
1.00	4.567	3.639	.945
1.50	4.804	3.779	1.390
2.00	5.007	3.910	1.715
2.50	5.184	4.054	1.983
3.00	5.339	4.239	2.210
3.25	5.412	4.343	2.309
3.50	5.480	4.452	2.399
4.00	5.610	4.678	2.559
4.50	5.731	4.837	2.683
5.00	5.844	4.943	2.779
5.50	5.951	5.004	2.849
6.00	6.051	5.023	2.887
6.50	6.145	5.004	2.900
7.00	6.233	4.952	2.900
7.50	6.316	4.874	2.900
8.00	6.392	4.773	2.900
8.50	6.465	4.654	2.900
8.75	6.501	4.590	2.900
9.75	6.627	4.360	- - -
9.97	6.651	4.360	- - -
10.00	[1]6.568	4.360	- - -
10.50	[1]6.665	4.360	- - -
11.00	[1]6.744	4.360	- - -
11.50	6.801	4.360	- - -
12.00	6.841	4.360	- - -
12.50	6.876	4.360	- - -
13.00	6.906	4.360	- - -
13.50	6.932	4.360	- - -
14.00	6.954	4.360	- - -
14.50	6.973	4.360	- - -
15.00	6.987	4.360	- - -
15.50	6.996	4.360	- - -
16.00	7.000	4.360	- - -
16.38	7.000	4.360	- - -

[1]These radii which form the cowl-gap exit are smaller than the NACA 1-series radii.
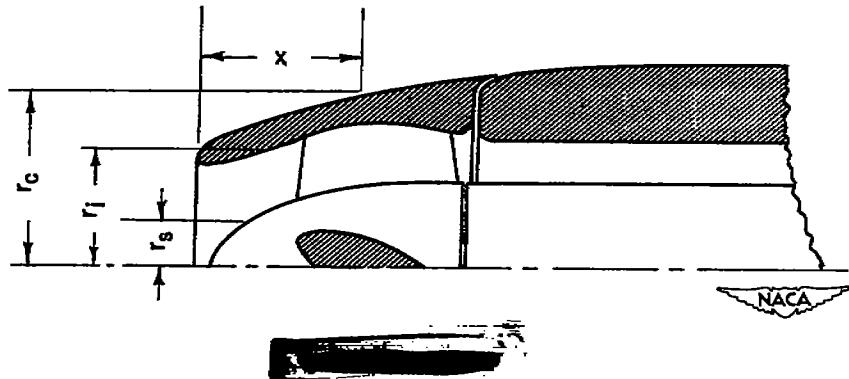
TABLE II.- BLADE-SHANK FAIRING COORDINATES AND TWIST

Coordinates		Twist	
Distance x, in.	Distance y, in.	Radius from center of rotation, in.	Angle from plane of rotation, β, deg
0	0	2.1	76.1
.07	.152	2.2	75.4
.14	.222	2.4	74.2
.28	.325	2.6	72.9
.42	.407	2.8	71.7
.56	.475	3.0	70.5
.84	.586	3.2	69.3
1.12	.670	3.4	68.1
1.68	.782	3.6	67.0
2.24	.834	3.8	65.8
2.52	.840	4.0	64.7
2.80	.834	4.2	63.6
3.36	.786	4.4	62.6
3.92	.682	4.6	61.5
4.48	.524	4.8	60.5
5.04	.303	5.0	59.5
5.32	.168	5.2	58.5
5.60	.017		
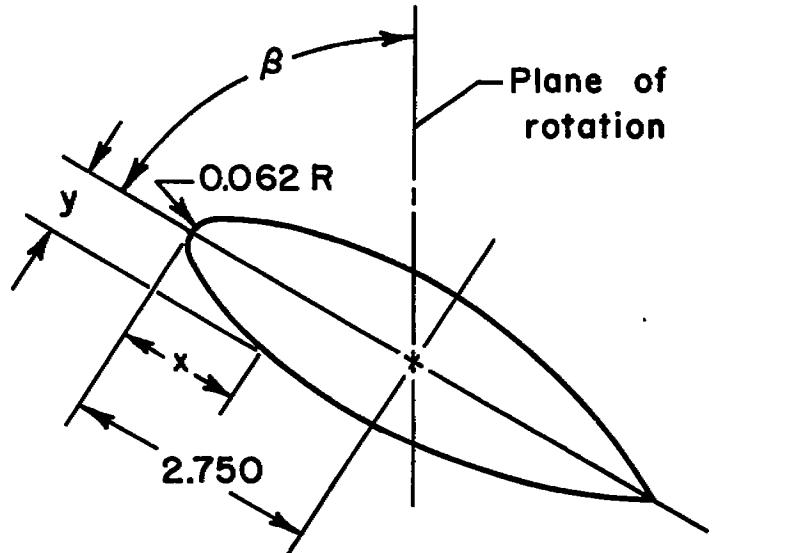
TABLE III.- LOCAL VELOCITY RATIO IN THE PROPELLER PLANE; U/V

Radial station, in.	M₀ = 0.20 — Inlet velocity ratio							M₀ = 0.40 — Inlet velocity ratio					M₀ = 0.60 — Inlet velocity ratio				
	0.23	0.32	0.40	0.56	0.73	0.87	0.94	0.30	0.40	0.55	0.72	0.86	0.20	0.29	0.38	0.70	0.81
6.30	1.094	1.094	1.095	1.085	1.080	1.075	1.069	1.101	1.096	1.089	1.084	1.079	1.114	1.111	1.104	1.093	1.092
6.55	1.094	1.094	1.095	1.085	1.080	1.075	1.074	1.101	1.099	1.089	1.086	1.081	1.116	1.112	1.105	1.095	1.093
6.80	1.093	1.093	1.089	1.084	1.074	1.074	1.068	1.094	1.091	1.081	1.079	1.076	1.106	1.102	1.097	1.085	1.085
7.05	1.078	1.078	1.079	1.069	1.064	1.059	1.058	1.080	1.083	1.070	1.067	1.062	1.099	1.090	1.086	1.076	1.074
7.30	1.078	1.078	1.079	1.069	1.064	1.059	1.058	1.083	1.085	1.072	1.067	1.062	1.099	1.088	1.086	1.074	1.074
7.80	1.062	1.062	1.058	1.053	1.048	1.048	1.042	1.067	1.067	1.060	1.055	1.051	1.088	1.080	1.073	1.062	1.061
8.30	1.067	1.062	1.063	1.058	1.048	1.048	1.042	1.065	1.067	1.057	1.055	1.051	1.086	1.074	1.069	1.061	1.061
8.80	1.056	1.056	1.052	1.047	1.042	1.042	1.036	1.059	1.056	1.051	1.046	1.041	1.080	1.068	1.062	1.055	1.055
9.30	1.046	1.046	1.047	1.042	1.037	1.031	1.031	1.049	1.049	1.041	1.036	1.033	1.069	1.059	1.055	1.047	1.047
10.30	1.040	1.040	1.041	1.036	1.025	1.030	1.025	1.038	1.038	1.033	1.028	1.026	1.059	1.047	1.043	1.036	1.036
11.30	1.029	1.029	1.035	1.024	1.019	1.019	1.014	1.037	1.035	1.030	1.027	1.025	1.057	1.047	1.045	1.036	1.036
12.30	1.029	1.024	1.029	1.024	1.019	1.019	1.014	1.031	1.031	1.026	1.024	1.021	1.048	1.044	1.041	1.039	1.035
13.30	1.023	1.023	1.023	1.018	1.013	1.013	1.013	1.024	1.021	1.019	1.016	1.014	1.032	1.030	1.027	1.022	1.023
15.30	1.022	1.017	1.022	1.022	1.012	1.012	1.022	1.018	1.020	1.018	1.020	1.018	1.022	1.018	1.020	1.020	1.022
17.30	1.011	1.011	1.011	1.006	1.006	1.006	1.001	1.014	1.011	1.011	1.011	1.009	1.017	1.015	1.010	1.007	1.008
19.30	1.010	1.010	1.010	1.010	1.005	1.005	1.005	1.008	1.008	1.005	1.005	1.003	1.017	1.014	1.012	1.007	1.010
21.30	1.010	1.010	1.010	1.010	1.005	1.010	1.000	1.004	1.007	1.004	1.004	1.002	1.013	1.011	1.009	1.006	1.009
23.30	1.009	1.009	1.009	1.009	1.004	1.009	.999	1.006	1.006	1.006	1.006	1.004	1.013	1.012	1.008	1.007	1.010
25.30	1.003	1.003	1.003	1.003	1.003	1.003	.998	1.005	1.005	1.002	1.002	1.000	1.011	1.009	1.006	1.004	1.006
27.30	1.013	1.013	1.013	1.013	1.008	1.013	1.008	1.006	1.006	1.006	1.006	1.005	1.009	1.007	1.005	1.002	1.005
29.30	1.003	1.003	1.008	1.003	1.008	1.003	.998	1.005	1.005	1.003	1.005	1.004	1.011	1.009	1.008	1.006	1.008
31.30	1.007	1.007	1.007	1.007	1.007	1.007	1.007	1.005	1.005	1.003	1.005	1.004	1.009	1.007	1.004	1.006	1.007
33.30	1.007	1.007	1.007	1.007	1.007	1.007	1.007	1.004	1.004	1.004	1.004	1.003	1.004	1.002	1.000	1.000	1.002
35.30	1.007	1.007	1.012	1.012	1.007	1.012	1.007	1.003	1.006	1.003	1.003	1.002	1.009	1.007	1.000	1.003	1.005

Radial station, in.	M₀ = 0.70 — Inlet velocity ratio						M₀ = 0.80 — Inlet velocity ratio						M₀ = 0.84 — Inlet velocity ratio			
	0.19	0.29	0.38	0.54	0.72	0.79	0.21	0.28	0.38	0.52	0.67	0.74	0.21	0.31	0.57	0.72
6.30	1.123	1.117	1.112	1.105	1.096	1.094	1.134	1.132	1.126	1.119	1.110	1.106	1.138	1.130	1.117	1.107
6.55	1.126	1.121	1.117	1.109	1.100	1.100	1.138	1.133	1.122	1.122	1.111	1.112	1.139	1.133	1.119	1.112
6.80	1.115	1.106	1.102	1.097	1.090	1.090	1.125	1.124	1.117	1.110	1.101	1.101	1.132	1.124	1.108	1.103
7.05	1.102	1.096	1.094	1.087	1.078	1.076	1.113	1.111	1.105	1.098	1.087	1.086	1.120	1.113	1.096	1.089
7.30	1.102	1.097	1.094	1.087	1.078	1.075	1.115	1.113	1.106	1.101	1.090	1.090	1.120	1.114	1.098	1.091
7.80	1.090	1.084	1.081	1.076	1.066	1.069	1.100	1.097	1.092	1.087	1.077	1.077	1.106	1.098	1.084	1.076
8.30	1.087	1.081	1.078	1.070	1.063	1.064	1.100	1.097	1.092	1.083	1.077	1.076	1.106	1.098	1.084	1.075
8.80	1.079	1.073	1.073	1.068	1.057	1.055	1.089	1.088	1.081	1.077	1.067	1.066	1.093	1.089	1.074	1.066
9.30	1.069	1.066	1.063	1.055	1.049	1.046	1.077	1.076	1.069	1.065	1.058	1.056	1.079	1.074	1.055	1.047
10.30	1.058	1.054	1.052	1.049	1.039	1.037	1.069	1.071	1.062	1.055	1.049	1.048	1.074	1.067	1.055	1.047
11.30	1.061	1.055	1.052	1.046	1.042	1.042	1.067	1.065	1.061	1.057	1.049	1.049	1.066	1.061	1.051	1.047
12.30	1.055	1.052	1.051	1.046	1.041	1.039	1.058	1.064	1.058	1.055	1.049	1.049	1.066	1.062	1.051	1.048
13.30	1.039	1.034	1.046	1.028	1.023	1.027	1.043	1.040	1.033	1.033	1.028	1.028	1.042	1.033	1.029	1.027
15.30	1.022	1.021	1.021	1.022	1.023	1.027	1.033	1.033	1.031	1.029	1.026	1.033	1.032	1.027	1.022	1.016
17.30	1.021	1.016	1.016	1.015	1.012	1.013	1.012	1.013	1.015	1.004	.991	.992	1.000	1.005	1.005	1.011
19.30	1.025	1.018	1.018	1.015	1.014	1.012	1.023	1.023	1.025	1.017	1.013	1.013	1.026	1.021	1.015	1.014
21.30	1.019	1.016	1.015	1.015	1.012	1.012	1.016	1.016	1.013	1.012	1.008	1.008	1.015	1.013	1.009	1.004
23.30	1.017	1.014	1.014	1.014	1.010	1.009	1.016	1.015	1.014	1.011	1.008	1.008	1.017	1.014	1.008	1.005
25.30	1.014	1.013	1.013	1.011	1.009	1.007	1.016	1.016	1.012	1.011	1.009	1.009	1.015	1.012	1.008	1.005
27.30	1.008	1.006	1.006	1.006	1.001	1.002	1.009	1.009	1.008	1.006	1.002	1.001	1.012	1.006	1.001	1.000
29.30	1.012	1.009	1.009	1.009	1.006	1.006	1.005	1.005	1.002	1.002	.999	.997	1.010	1.003	.998	.997
31.30	1.010	1.008	1.007	1.007	1.004	1.005	1.008	1.009	1.008	1.005	1.004	1.004	1.009	1.010	1.002	1.001
33.30	1.009	1.005	1.005	1.005	1.002	1.003	1.010	1.011	1.008	1.008	1.003	1.004	1.012	1.008	1.003	1.003
35.30	1.009	1.006	1.006	1.004	1.002	1.003	1.011	1.007	1.010	1.007	1.006	1.003	1.012	1.010	1.004	1.002

Length of NACA 1-51-117 cowl

16.38

Note: Dimensions shown in inches.

Sta.②

9.85

6.00

See detail 'A'

Sliding throttle

7.00

8.93

2.75

4.36

0.50

0.03

Sta. ③

2.90

Model center line

Sta. ①

NACA 0030-34.5
Propeller-blade-shank fairing

Ram-recovery and yaw rake location

NACA 1-41.43-042.86 spinner

To leading edge
of cowl

10.00

0.75

0.03

Detail 'A'

0.83

1.34

0.50

0.50

5.81

Duct area, sq. ft.

.30

.26

.22

Cowl gap
location

0 2 4 6 8 10 12 14

Distance from leading edge of cowl, in.

To model
center line

Figure 1.- Model arrangement and duct area distribution.
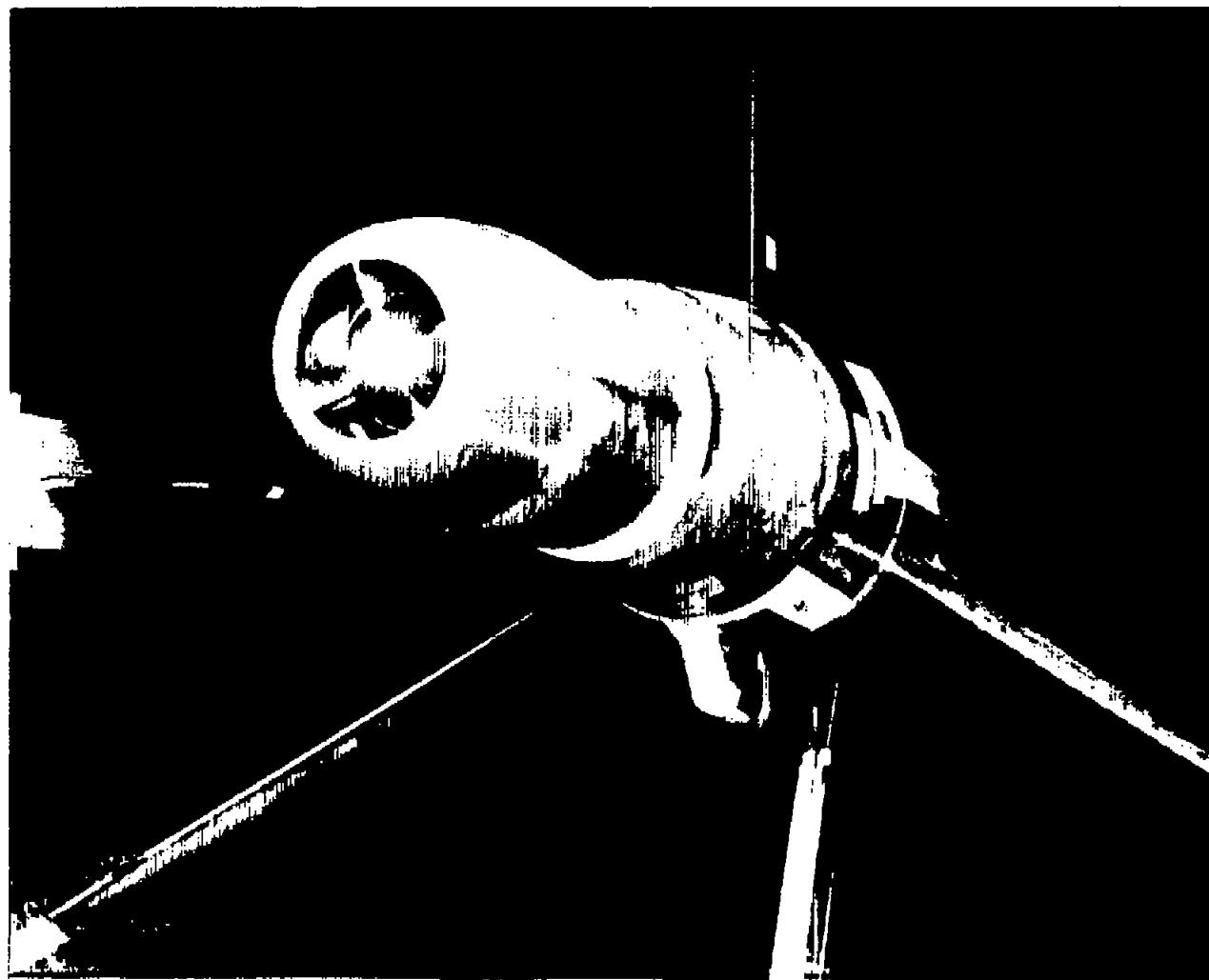
A-18436.1

Figure 2.- The model mounted on the 1000-horsepower dynamometer in the
12-foot pressure wind tunnel.
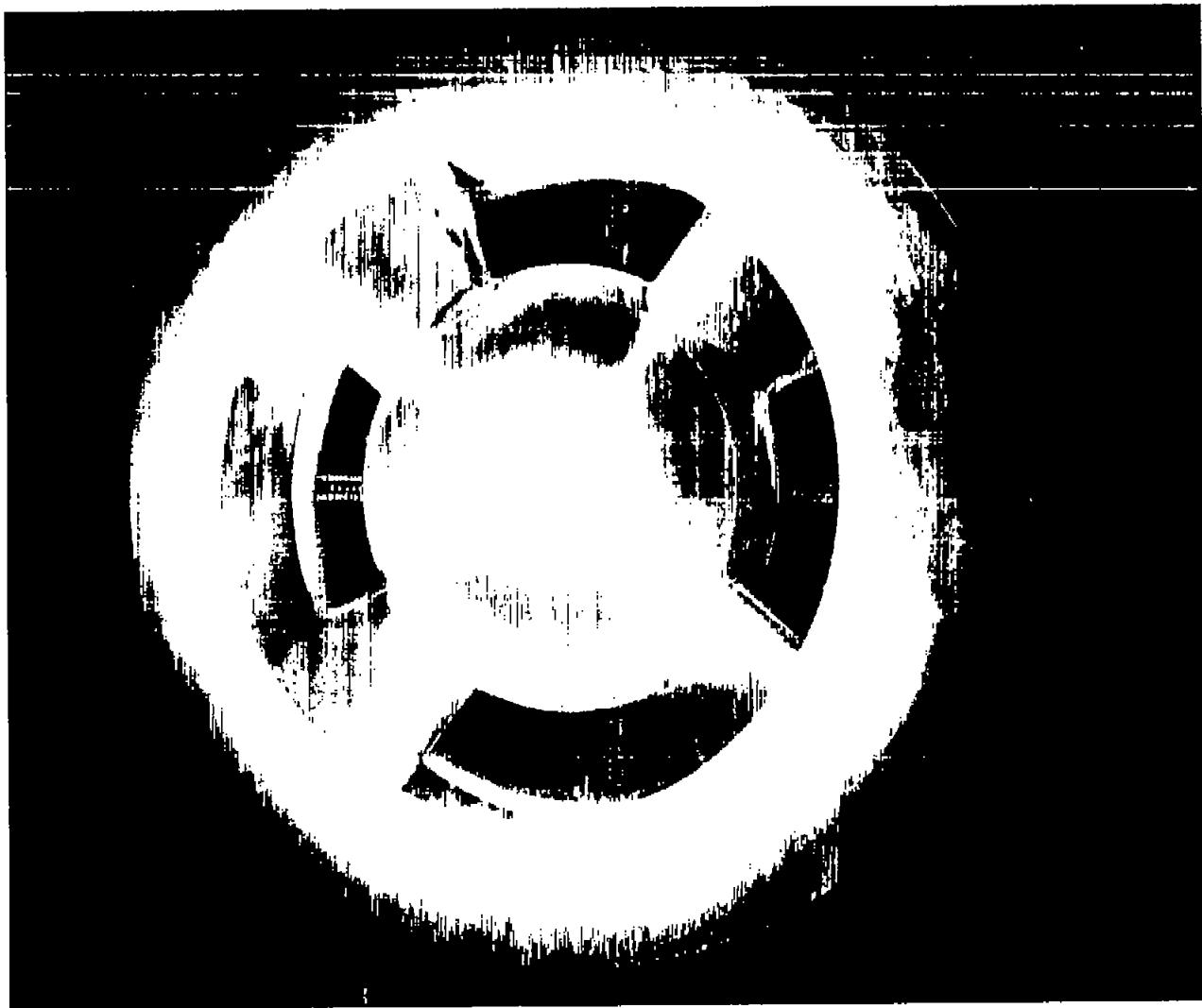
A-18437.1

Figure 3.- Close-up of the model showing the blade-shank fairings
and the total-pressure rakes.

.09r

50° (Typ)

See detail ⓐ

.002

20° chamfer

.040 O.D. hard
drawn stainless
steel tubing
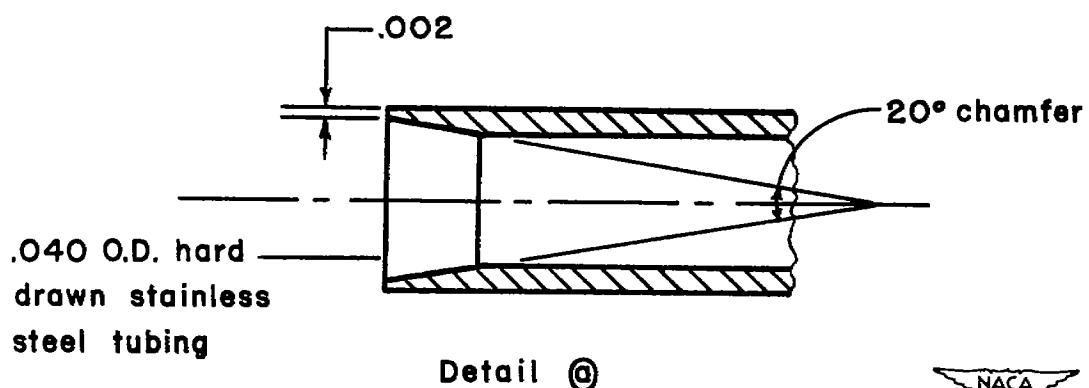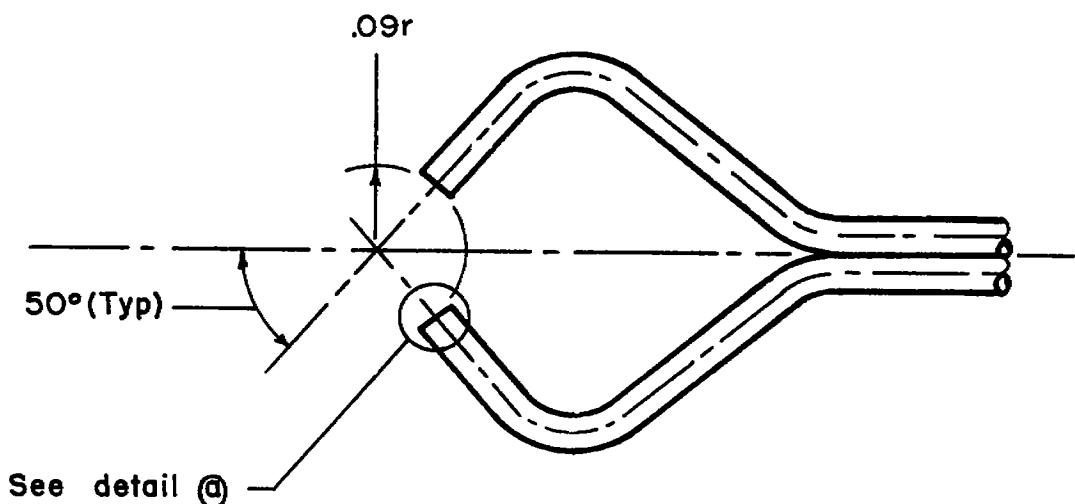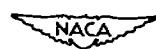
Detail ⓐ

NACA

Figure 4.- Yaw head details.
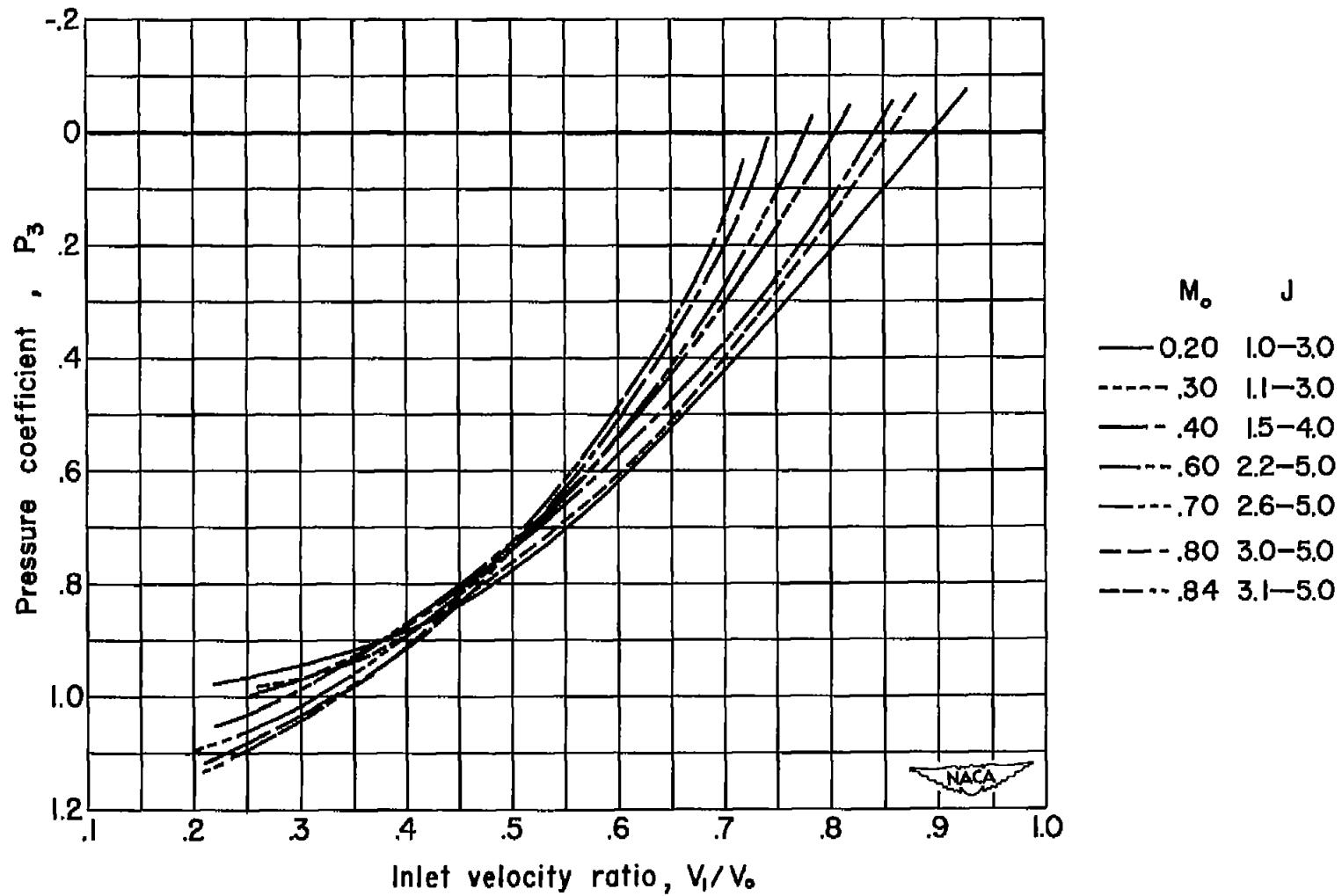
Figure 5.- The effect of inlet velocity ratio on the average pressure coefficient in the duct.

(a) $M_0 = 0.20$ (b) $M_0 = 0.30$
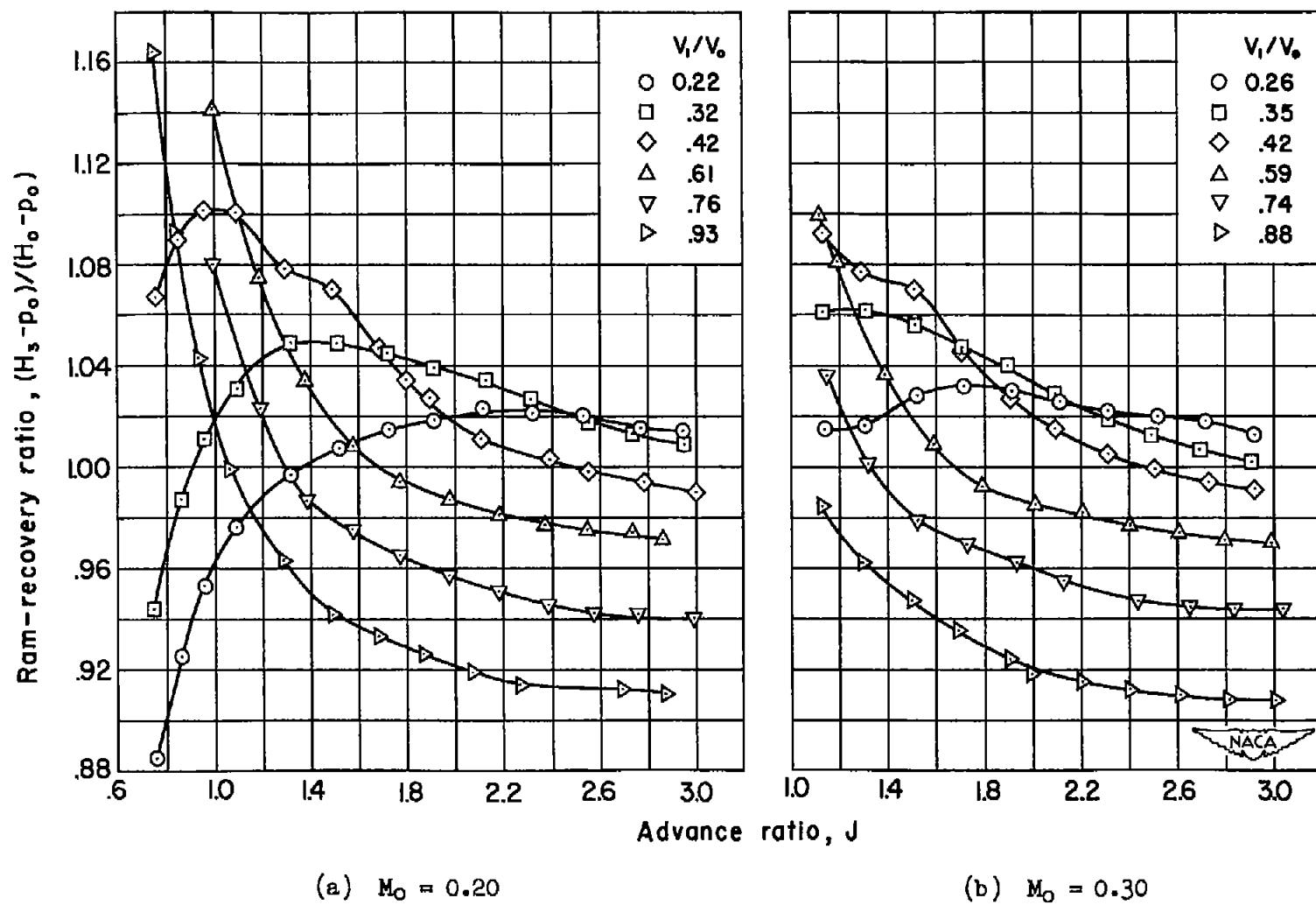
Figure 6.- The effect of advance ratio on the average ram-recovery ratio.

(c) $M_O = 0.40$

(d) $M_O = 0.60$
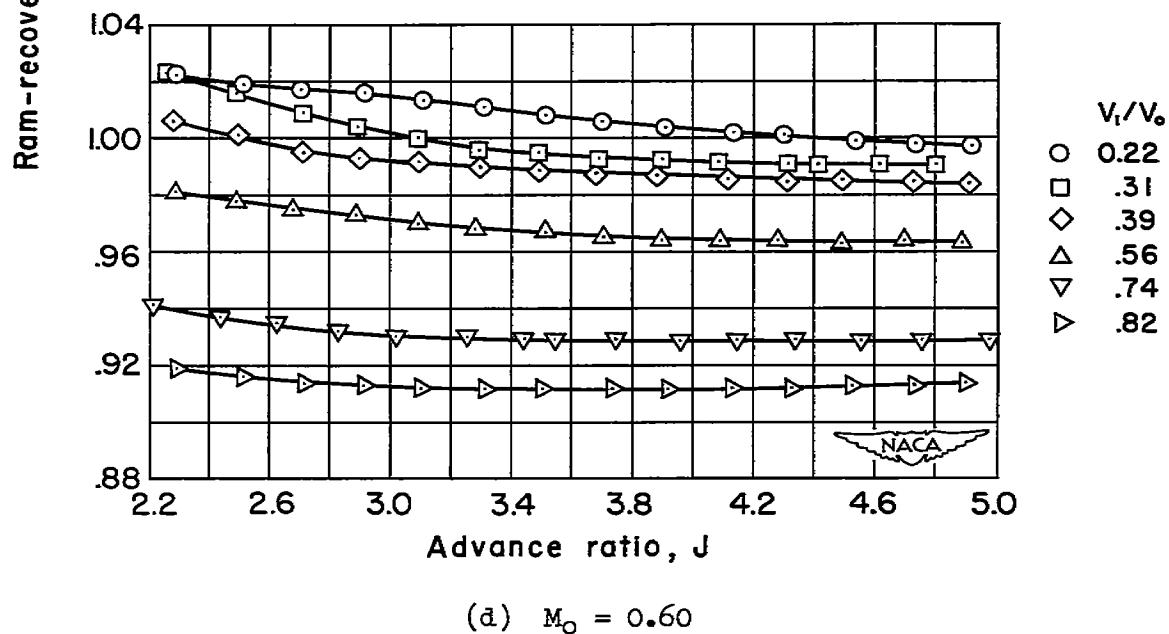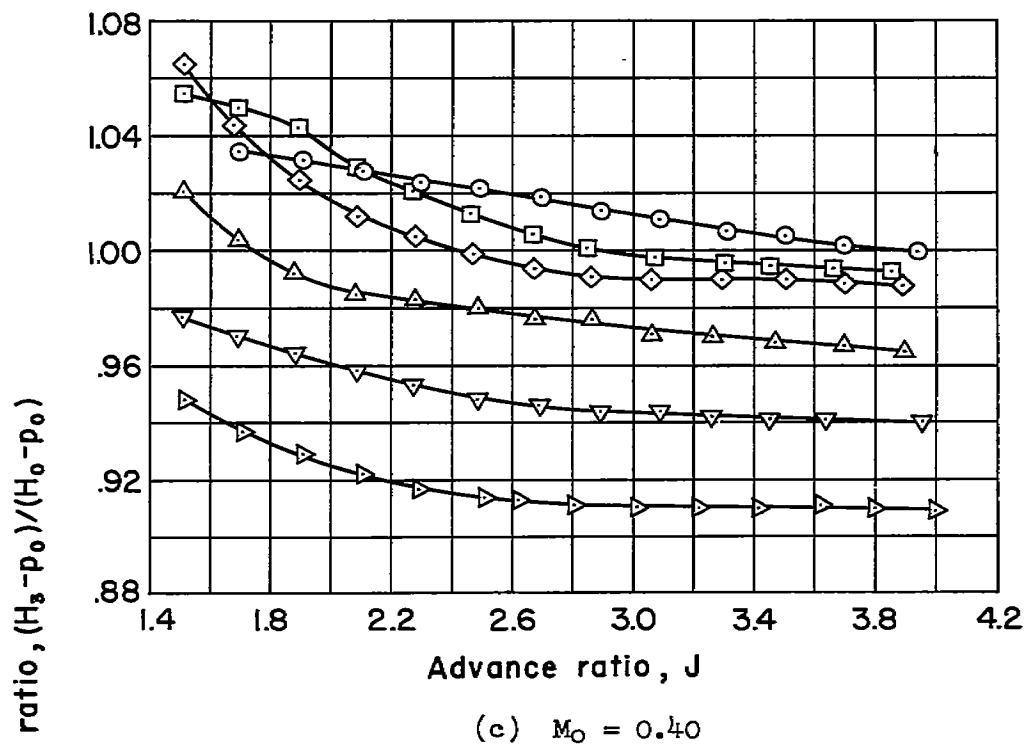
Figure 6.- Continued.

(e) $M_O = 0.70$

(f) $M_O = 0.80$

(g) $M_O = 0.84$
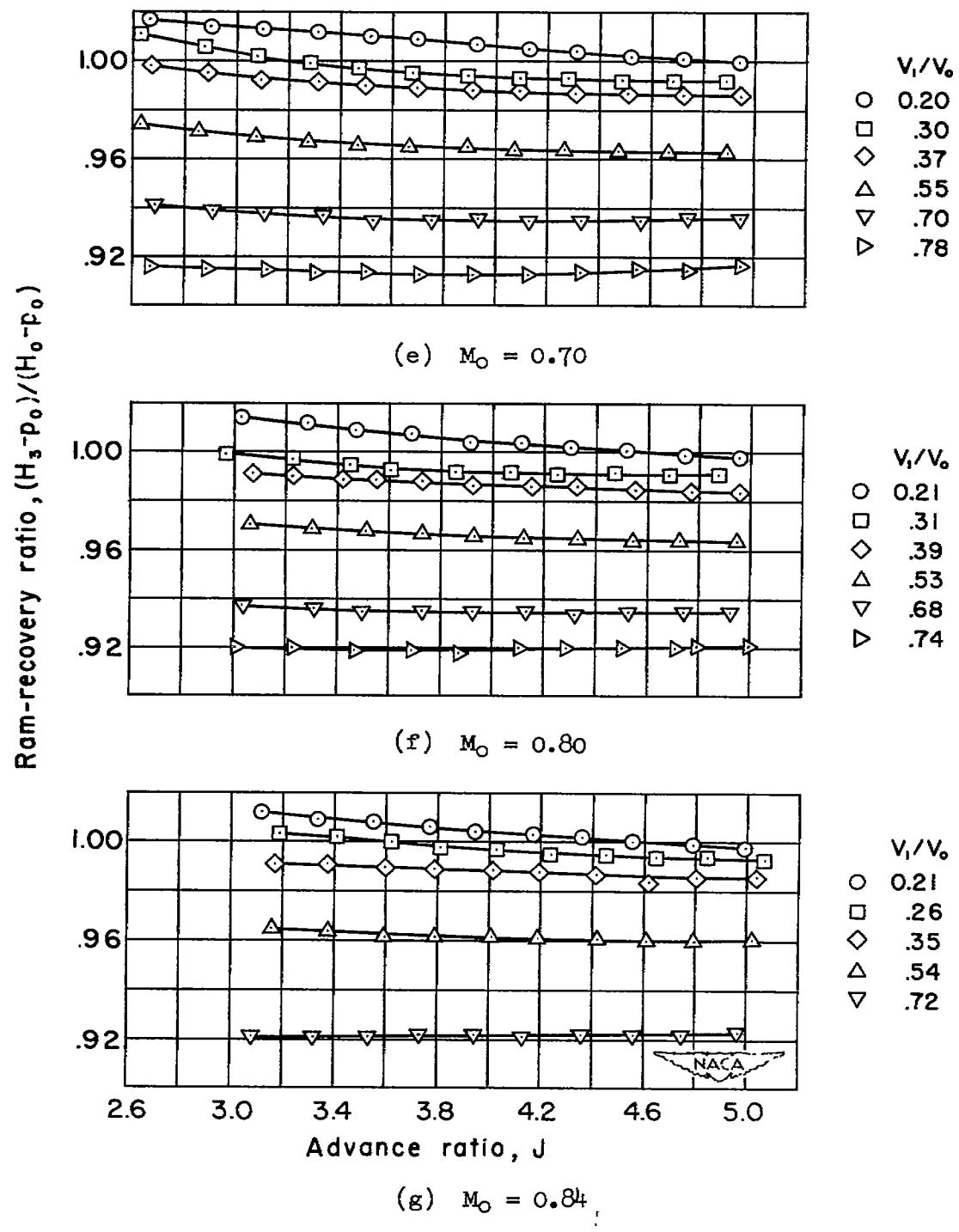
Figure 6.- Concluded.

(1) NACA I-series E-type cowling , rotating
(2) NACA I-series E-type cowling , nonrotating (ref. 2)
(3) NACA I-series D-type cowling , platform junctures (ref. 3)

(a)   J = 2.0
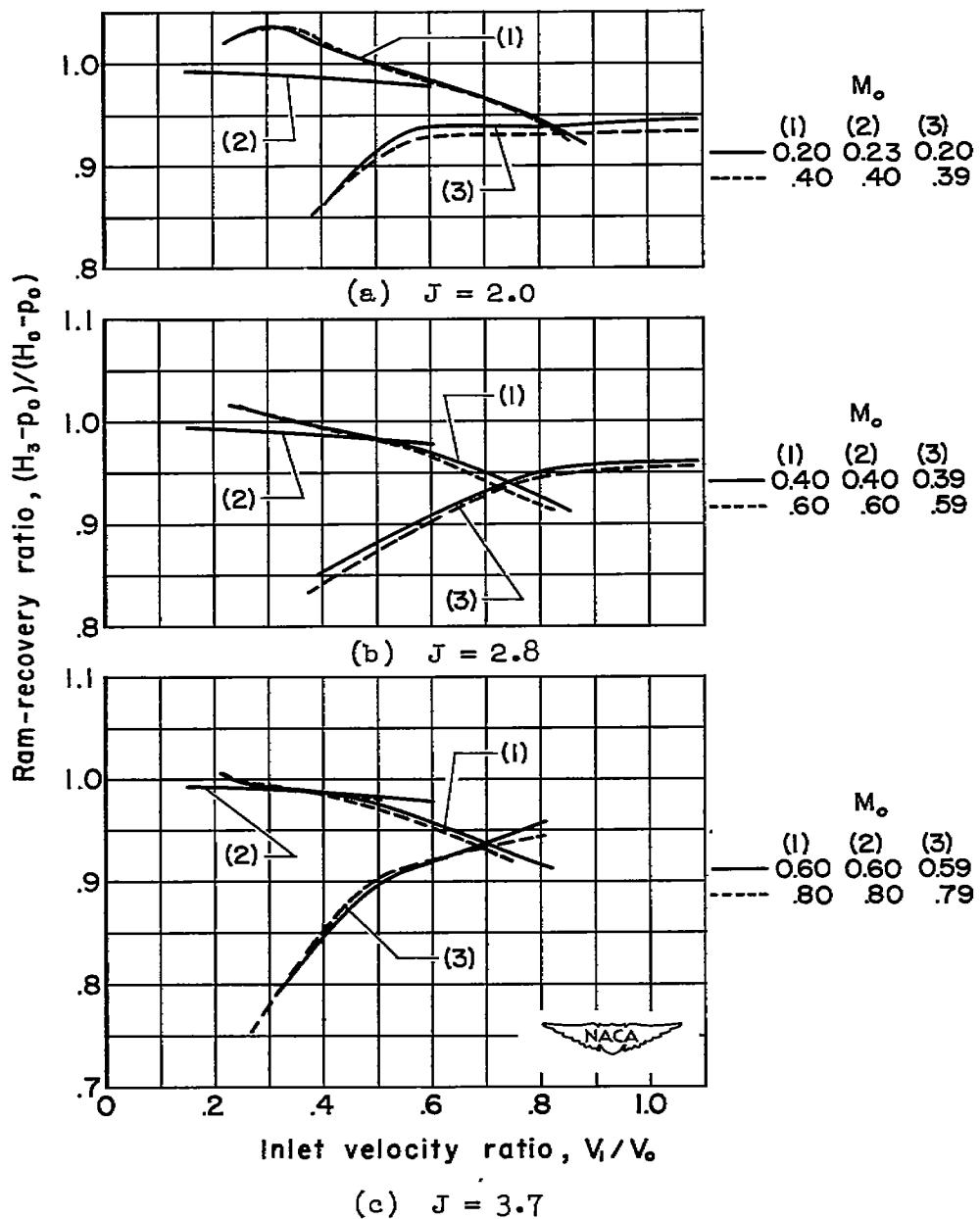
(b)   J = 2.8

(c)   J = 3.7

Figure 7.- The effect of inlet velocity ratio on the average
ram-recovery ratio.

(a) J = 2.0
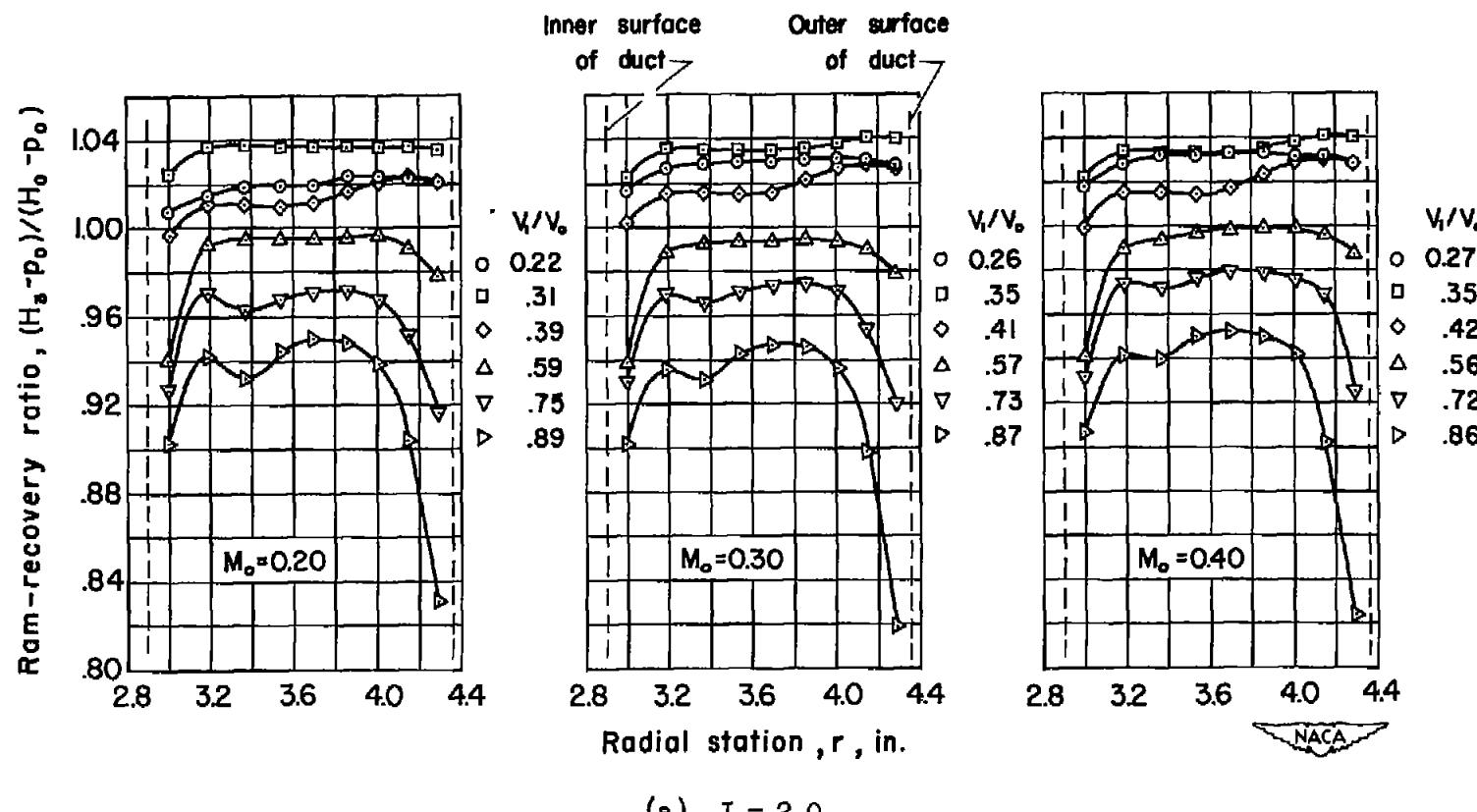
Figure 8.- The variation of the average ram-recovery ratio across the duct.
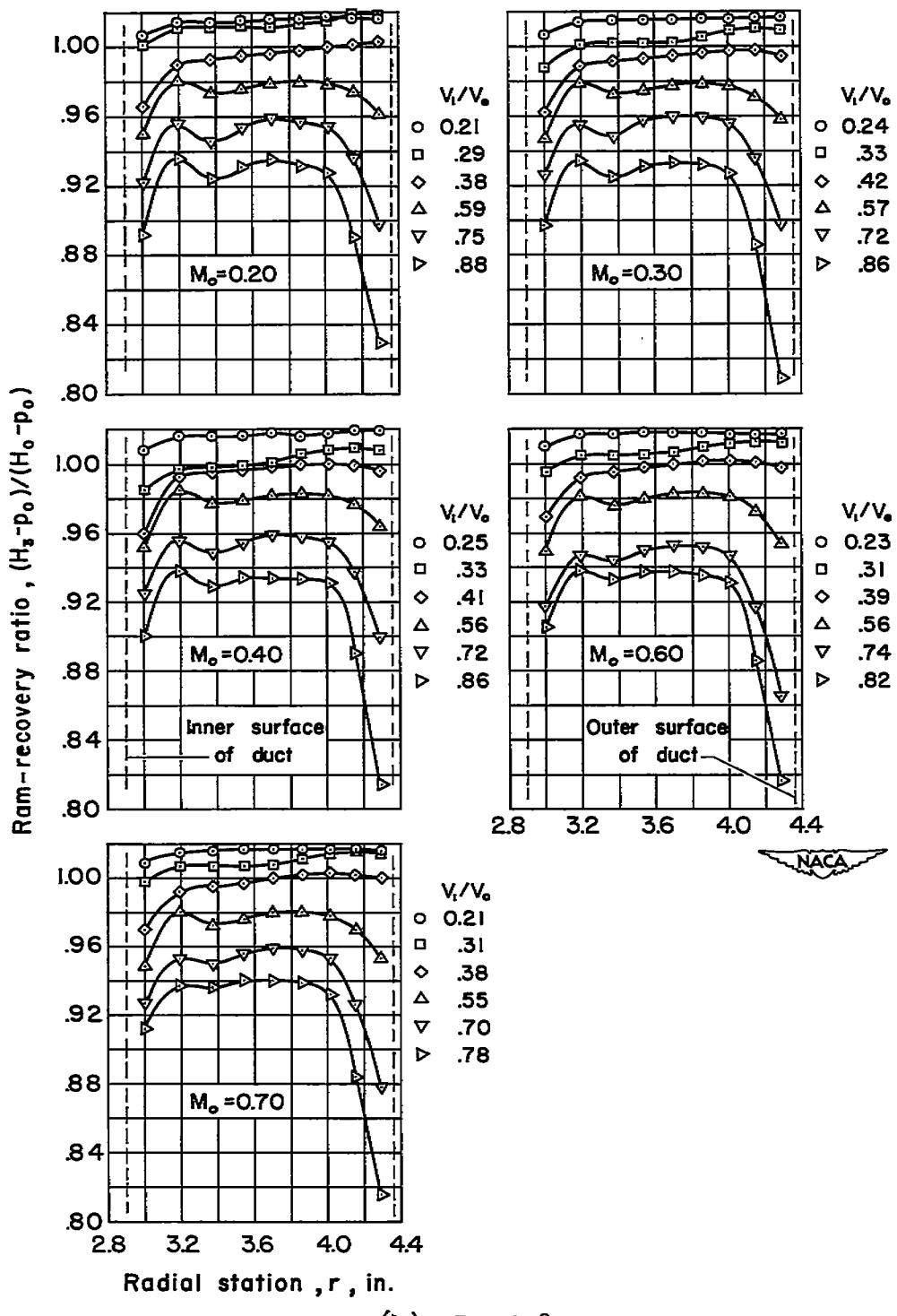
(b) $J = 2.8$

Figure 8.- Continued.
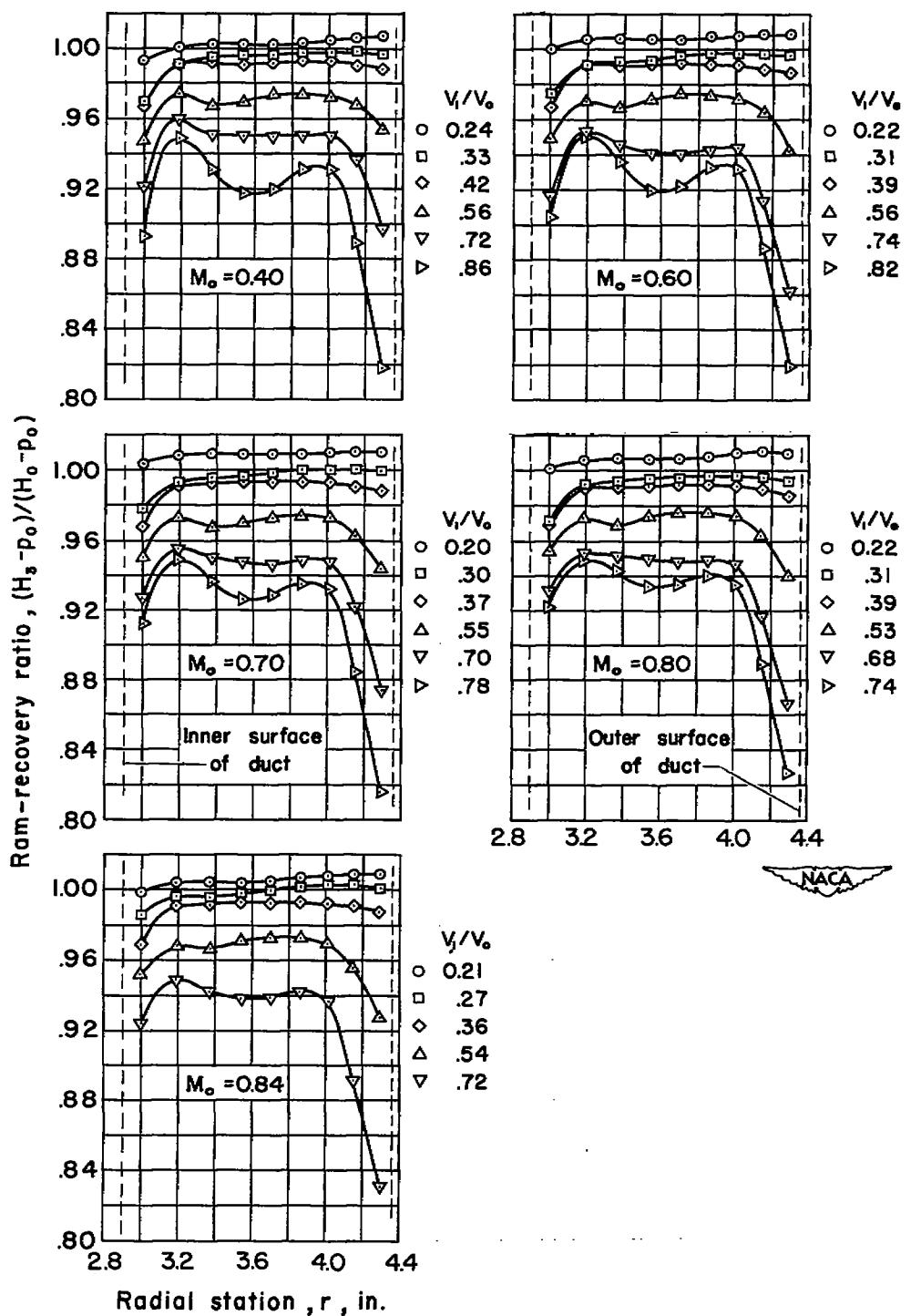
(c)   J = 3.7

Figure 8.- Concluded.
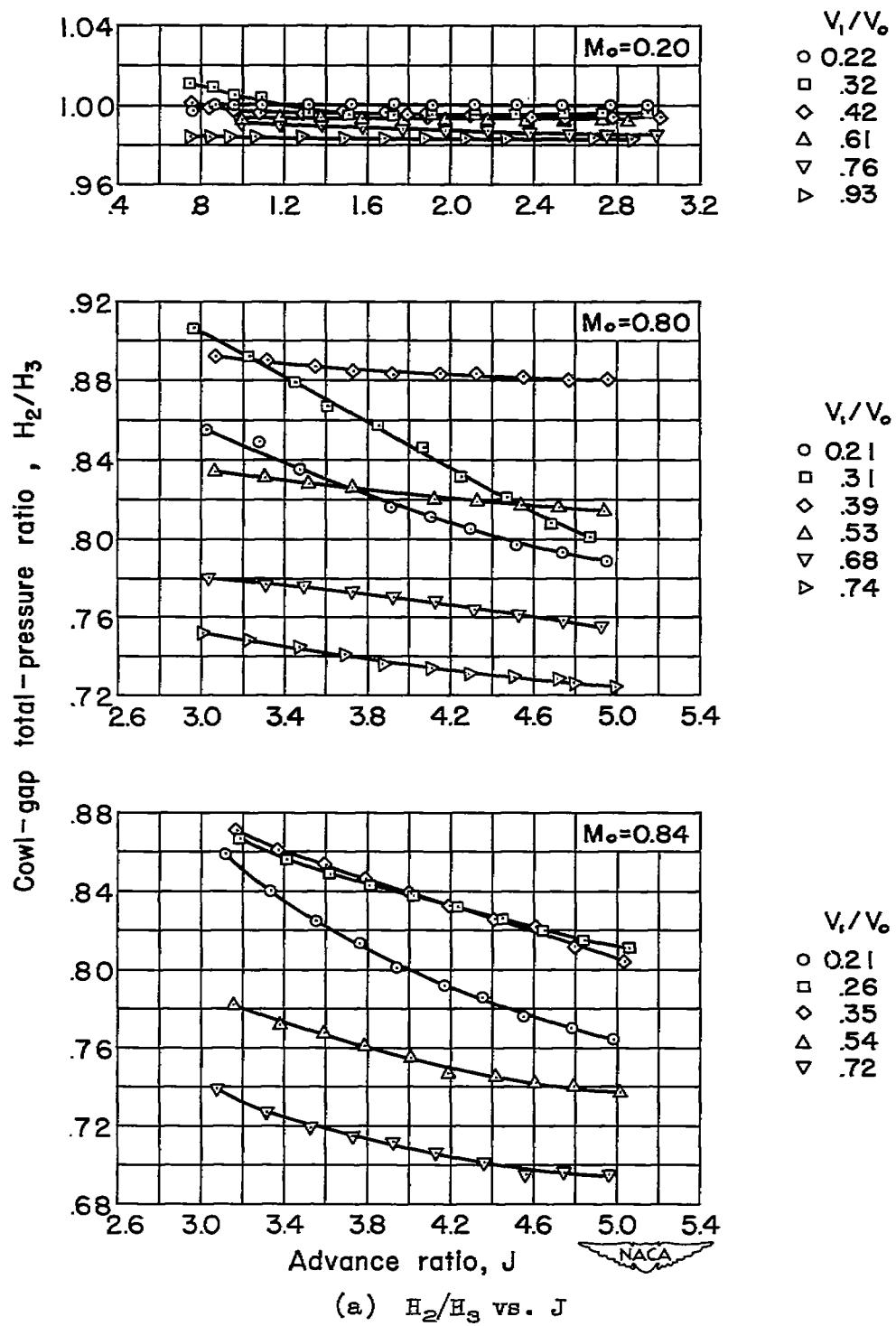
(a) H_2/H_3 vs. J

Figure 9.- Typical characteristics of the flow in the gap between the
rotating and stationary portions of the cowl.

$M_o = 0.20$

V_1/V_o

○ 0.22
□ .32
◇ .42
△ .61
▽ .76
▷ .93

$M_o = 0.80$

Pressure coefficient , P_2

V_1/V_o

○ 0.21
□ .31
◇ .39
△ .53
▽ .68
▷ .74

$M_o = 0.84$

V_1/V_o

○ 0.21
□ .26
◇ .35
△ .54
▽ .72

Advance ratio, J

(b) P_2 vs. J
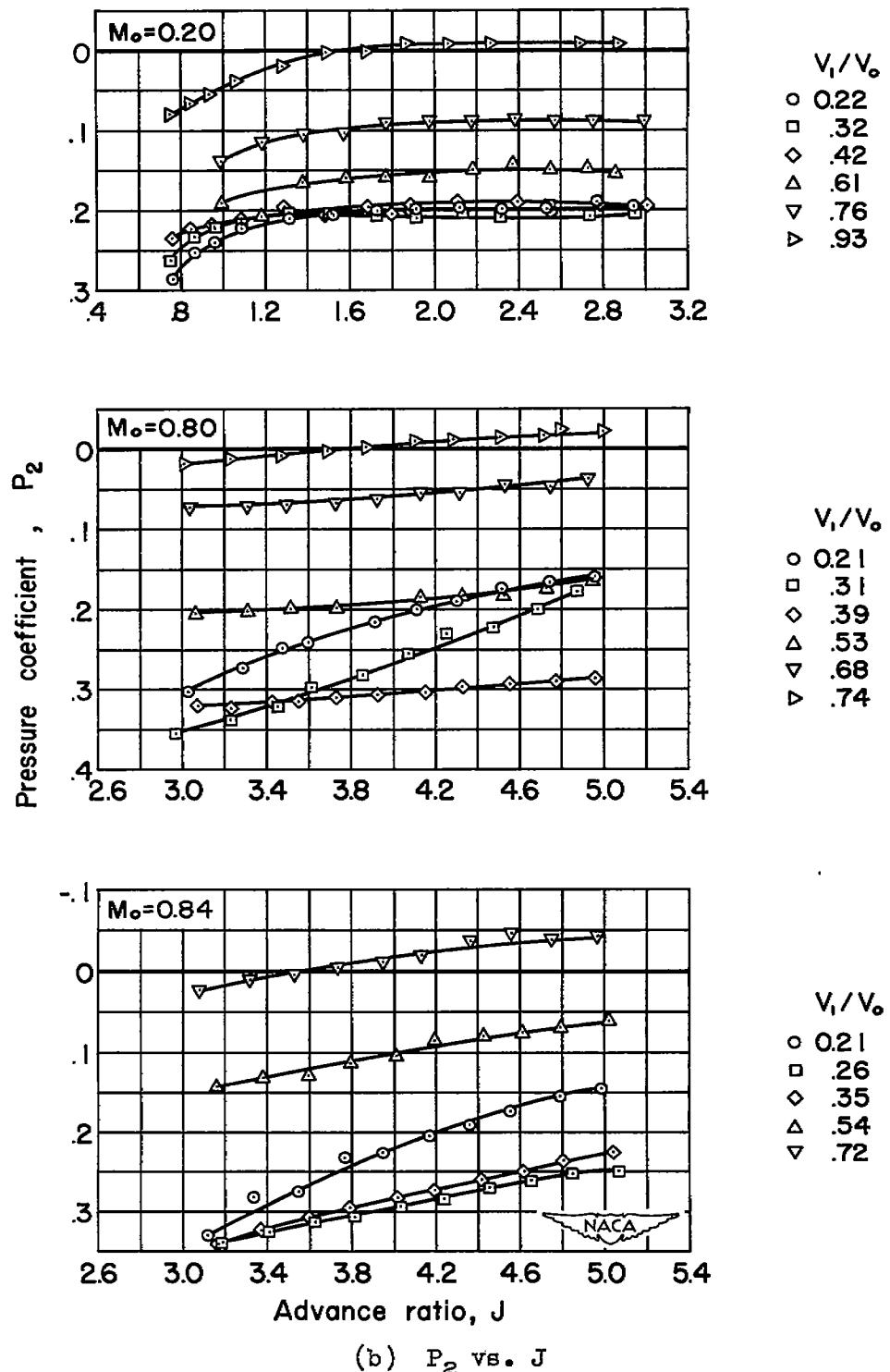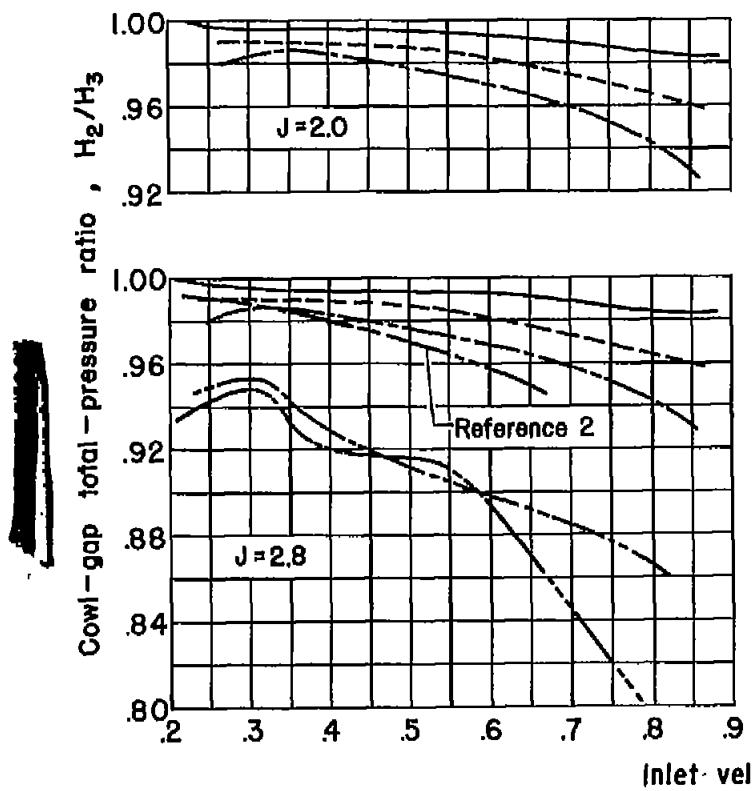
Figure 9.- Continued.

(c) H_2/H_3 vs. V_1/V_0

Figure 9.- Continued.

(d) P_2 vs. V_1/V_0
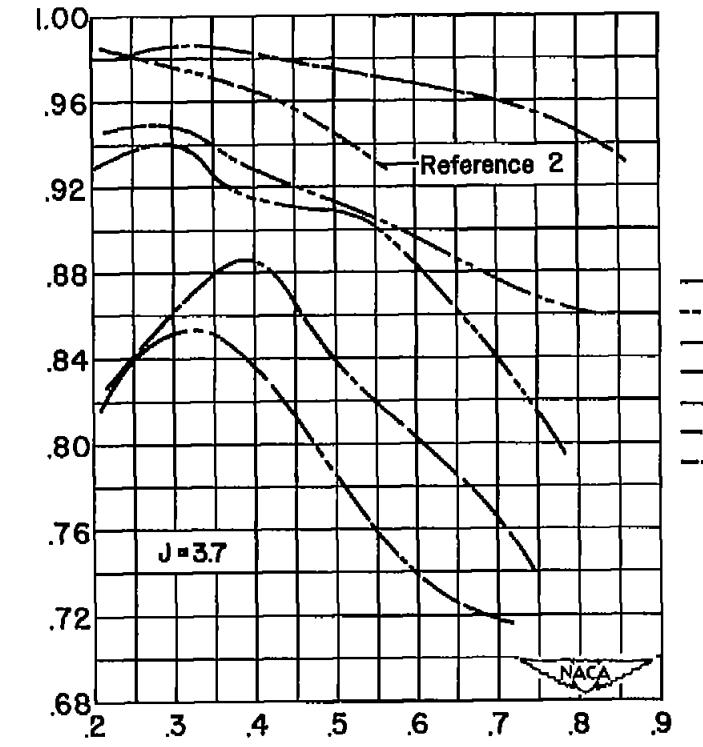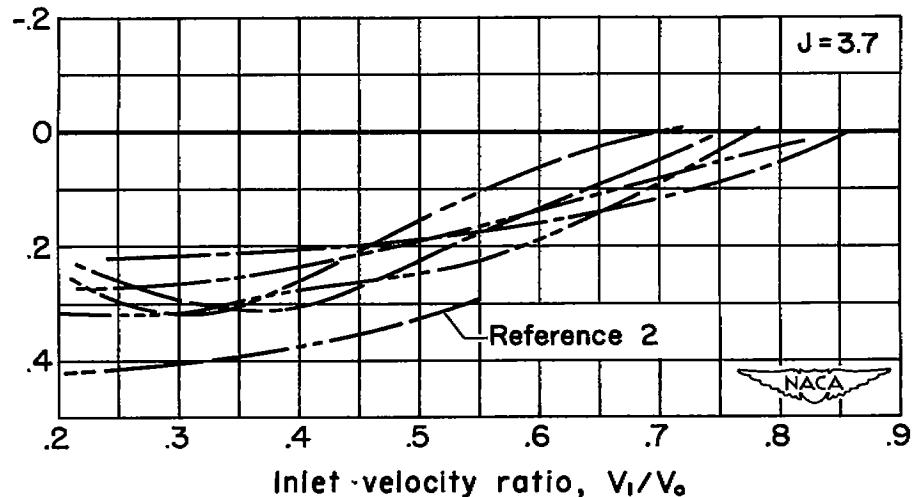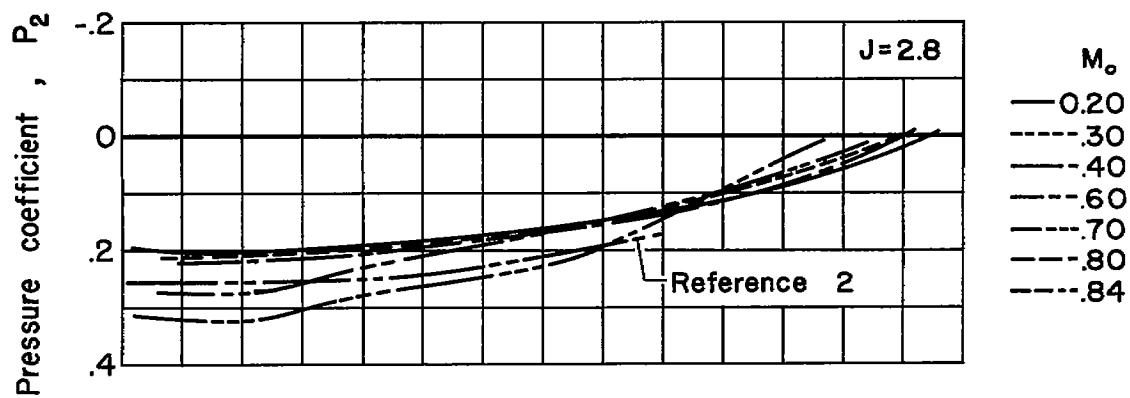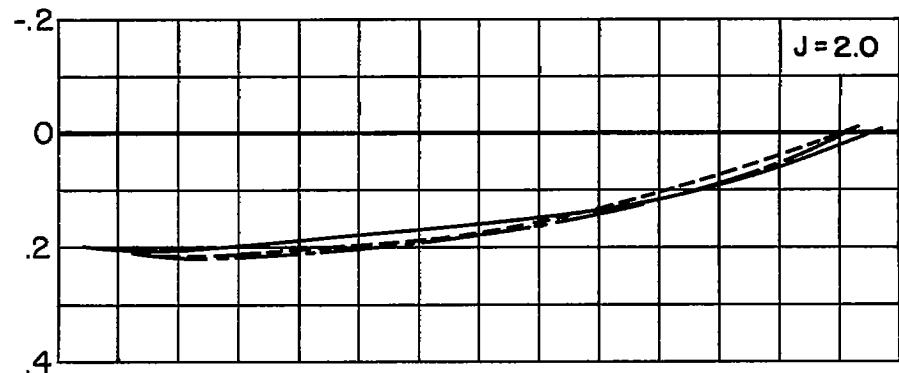
Figure 9.- Concluded.

(1) C_{D_g}-NACA I-series E-type cowl, rotating

(2) C_{D_g}-NACA I-series E-type cowl, nonrotating
(calculated from data of ref. 2)

(3) C_D -NACA I-series E-type cowl, nonrotating
(ref. 2)

(a)   J = 2.0

(b)   J = 2.8

(c)   J = 3.7
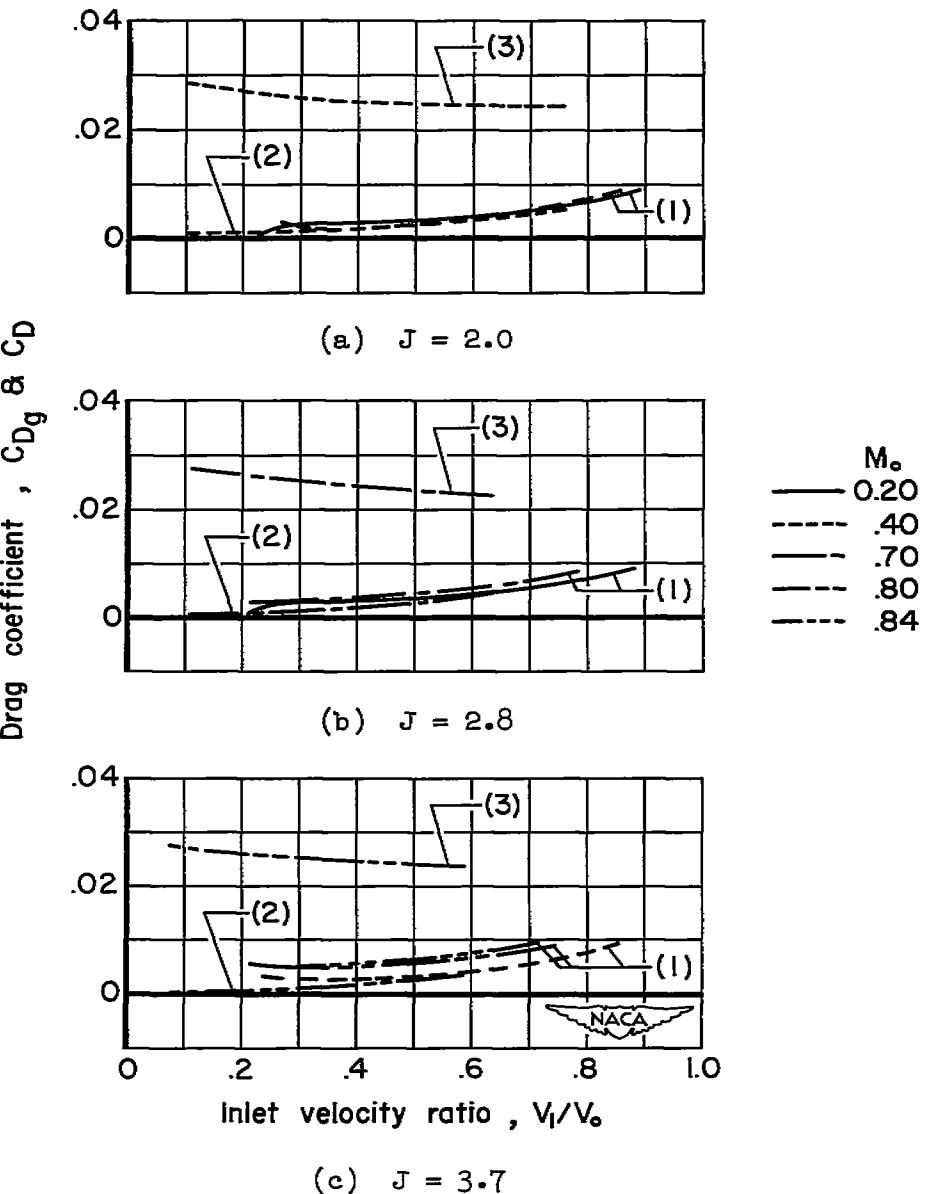
Figure 10.- The effect of inlet velocity ratio on the drag coefficient
due to the momentum loss in the air flow through the cowl gap (C_{D_g})
and on the external drag of the cowl (C_D).
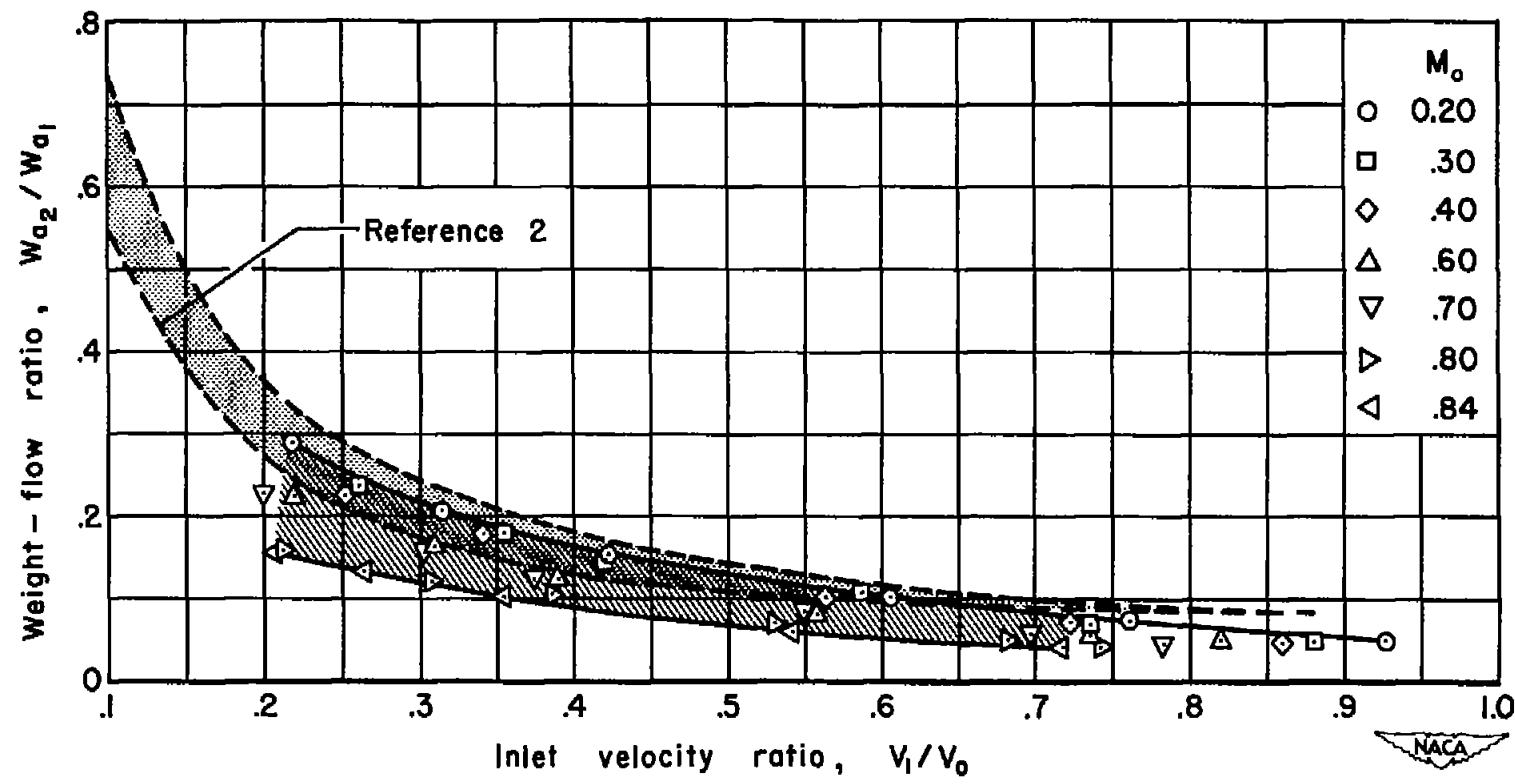
Figure 11.- The variation of the ratio of cowl-gap weight flow to inlet weight flow with inlet velocity ratio.

(a) M_O = 0.20
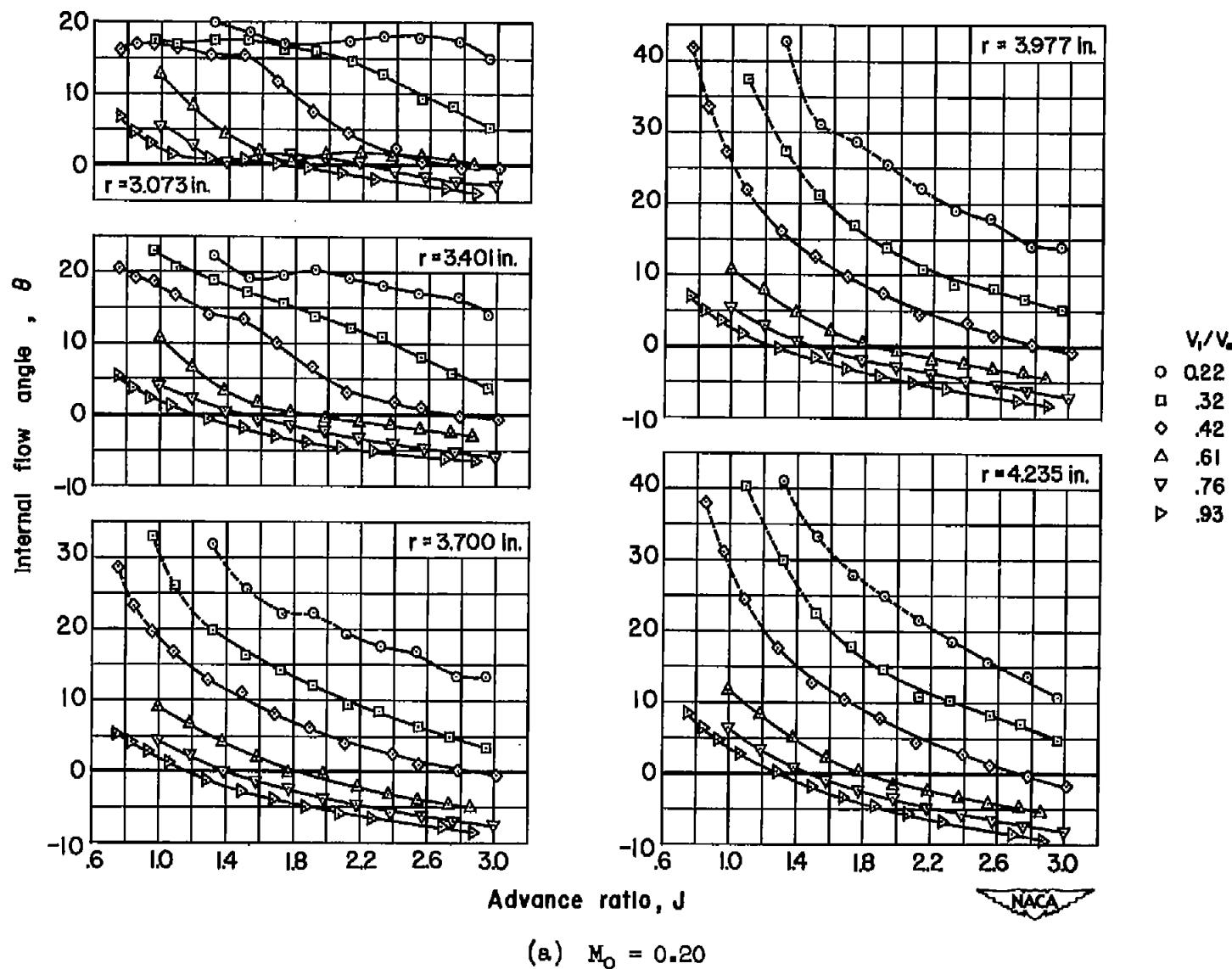
Figure 12.- The effect of advance ratio on the internal flow angle.

(b) $M_O = 0.30$

Figure 12.- Continued.

(c) $M_O = 0.40$
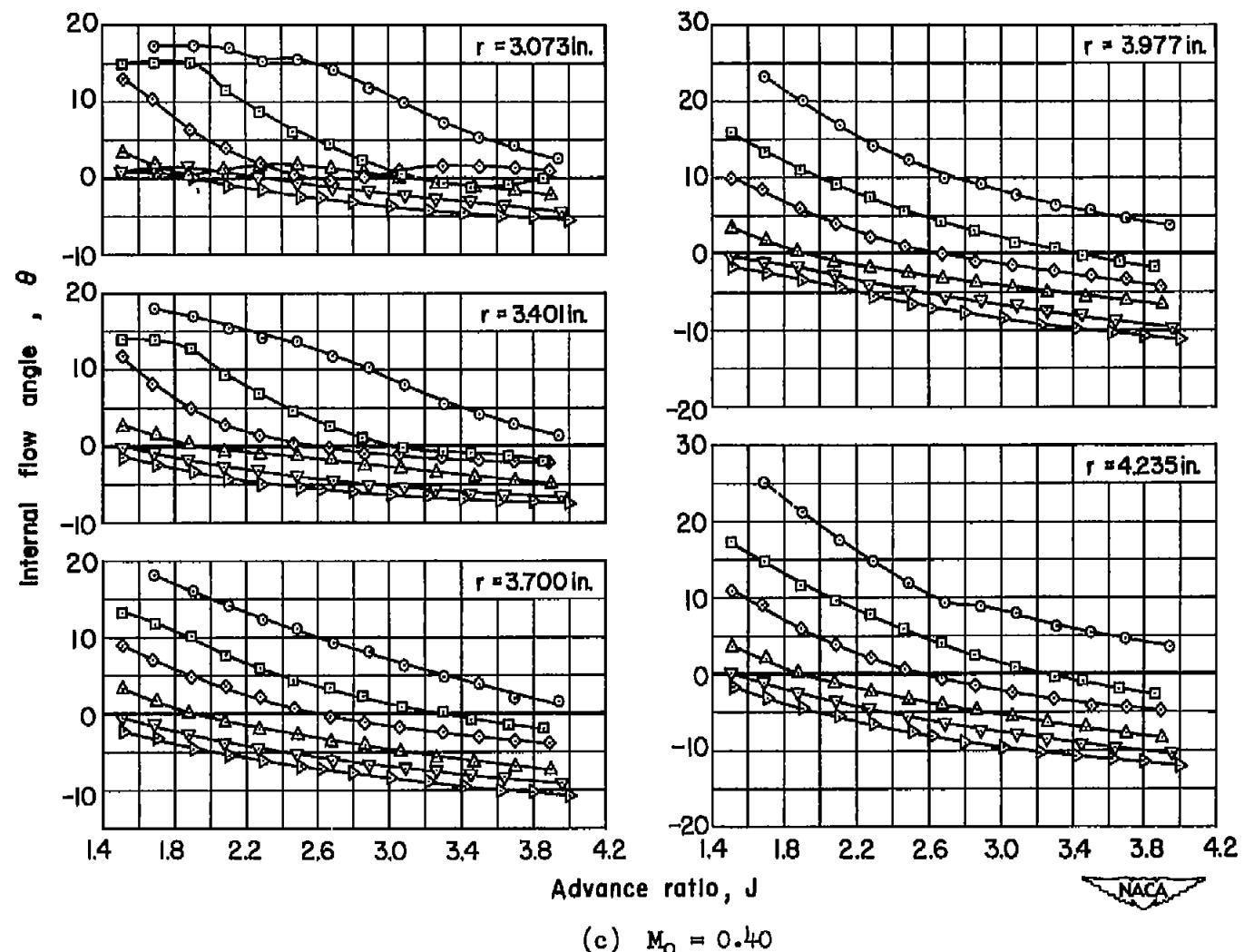
Figure 12.- Continued.
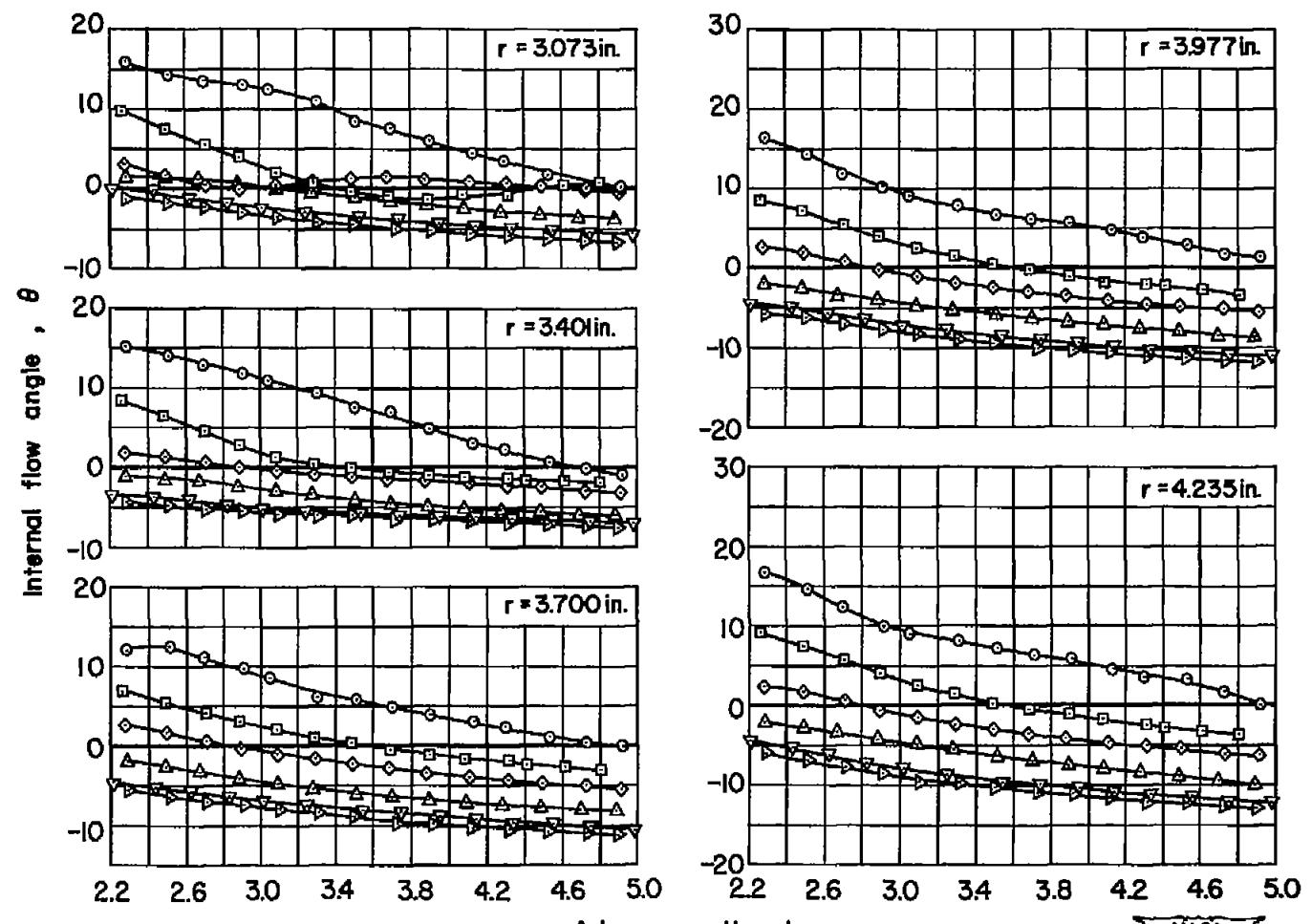
(d) $M_0 = 0.60$

Figure 12.- Continued.
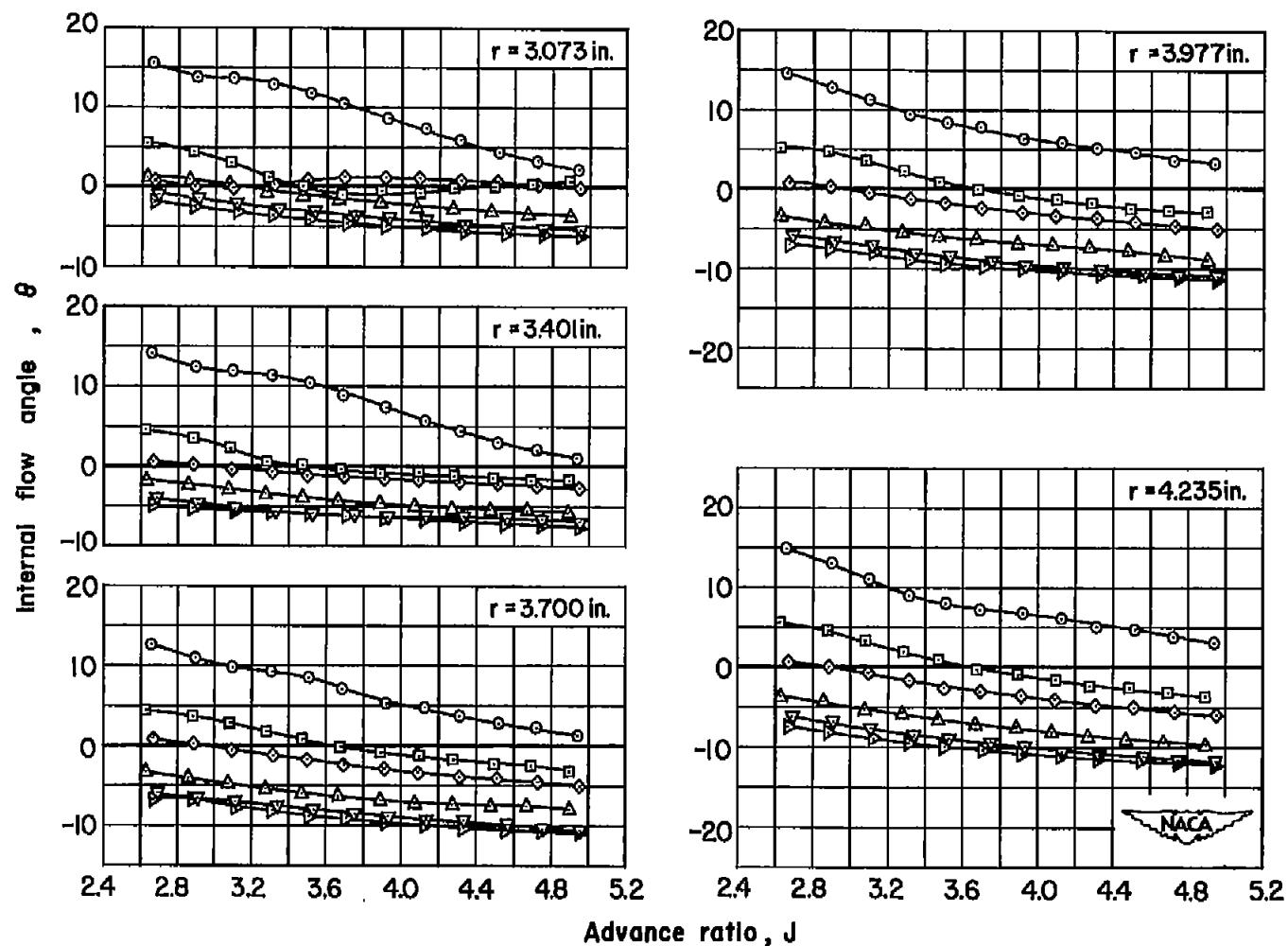
(e) $M_O = 0.70$

Figure 12.- Continued.

(f) $M_O = 0.80$
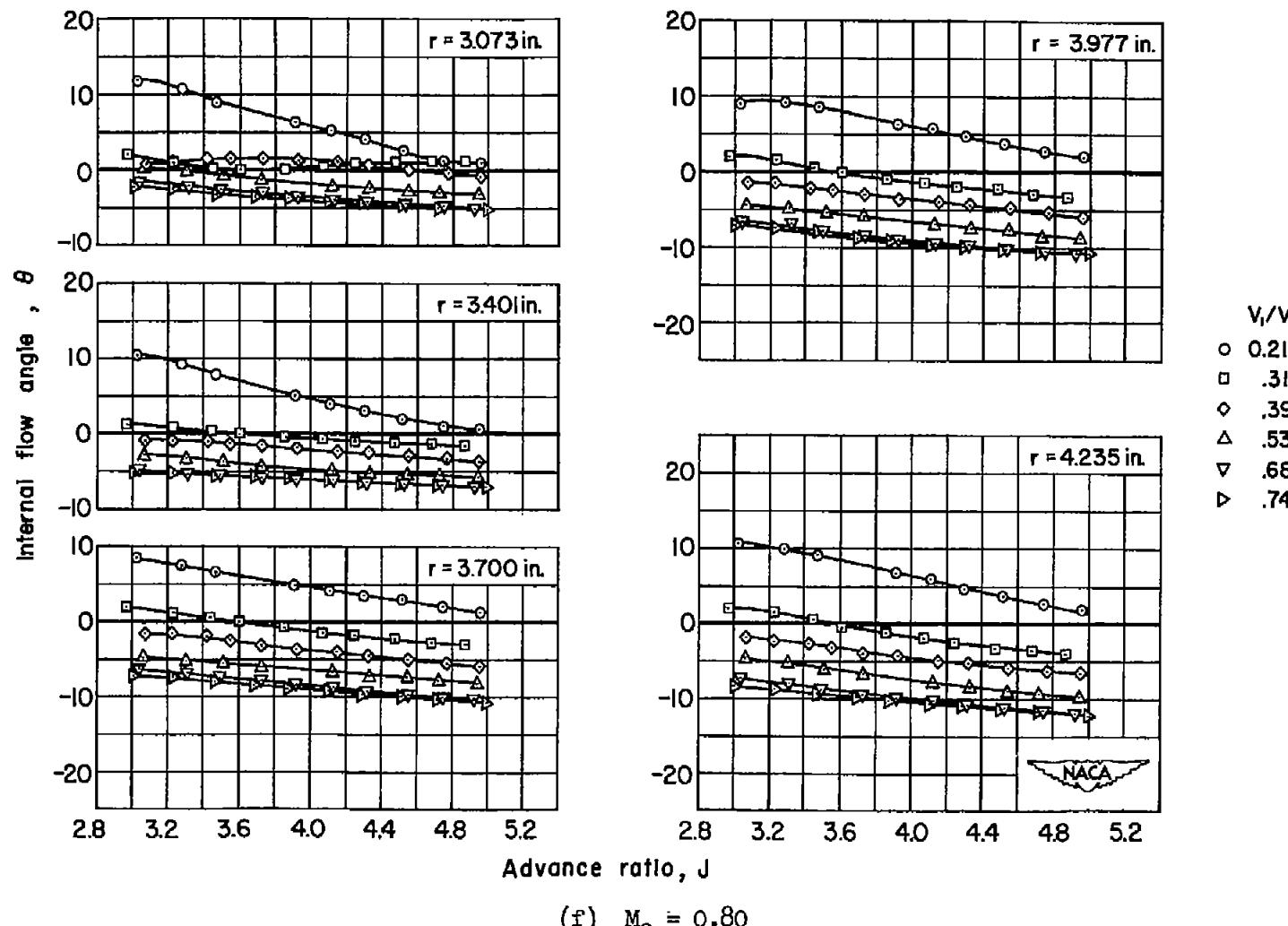
Figure 12.- Continued.
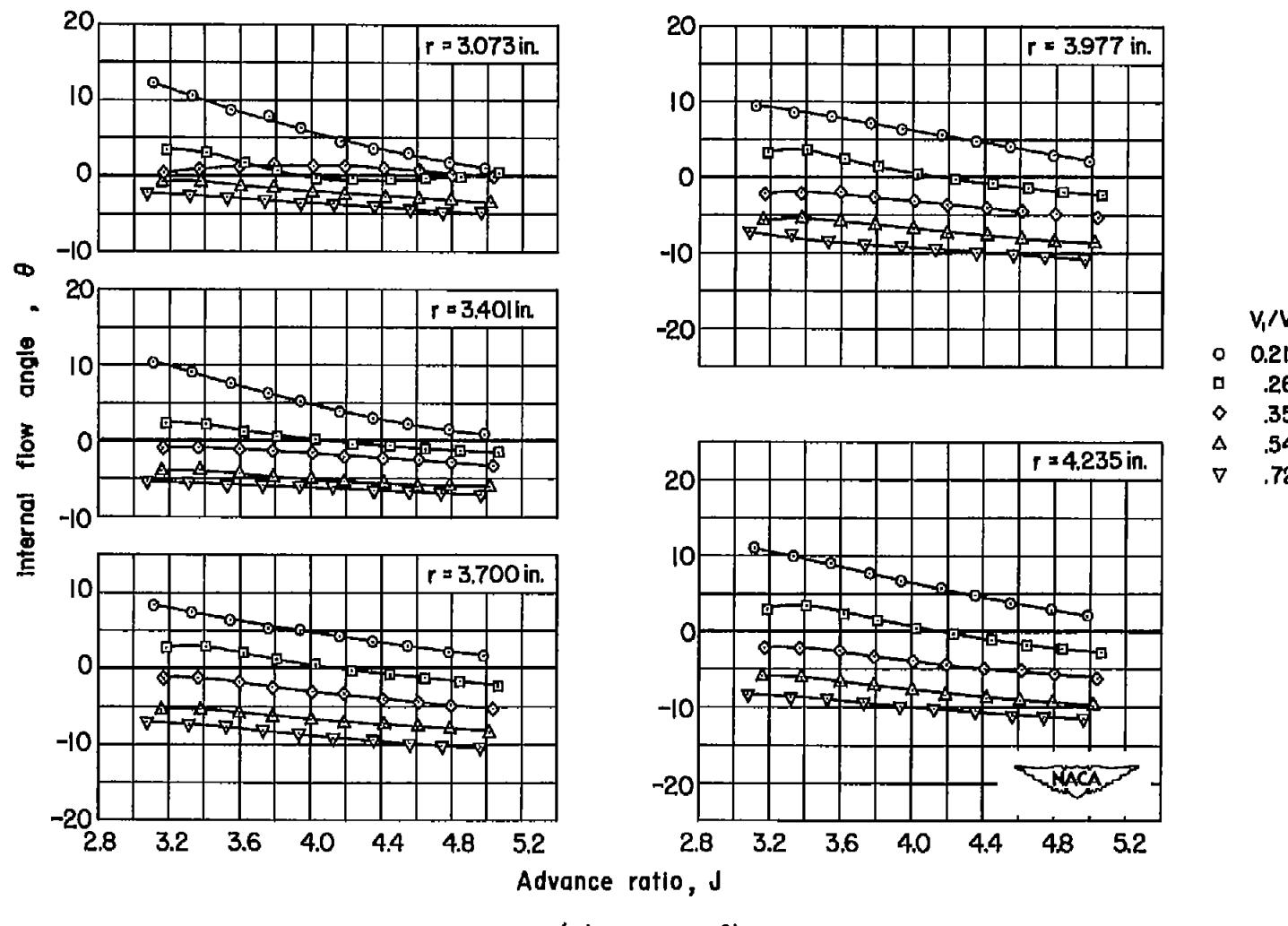
(g) $M_O = 0.84$

Figure 12.- Concluded.
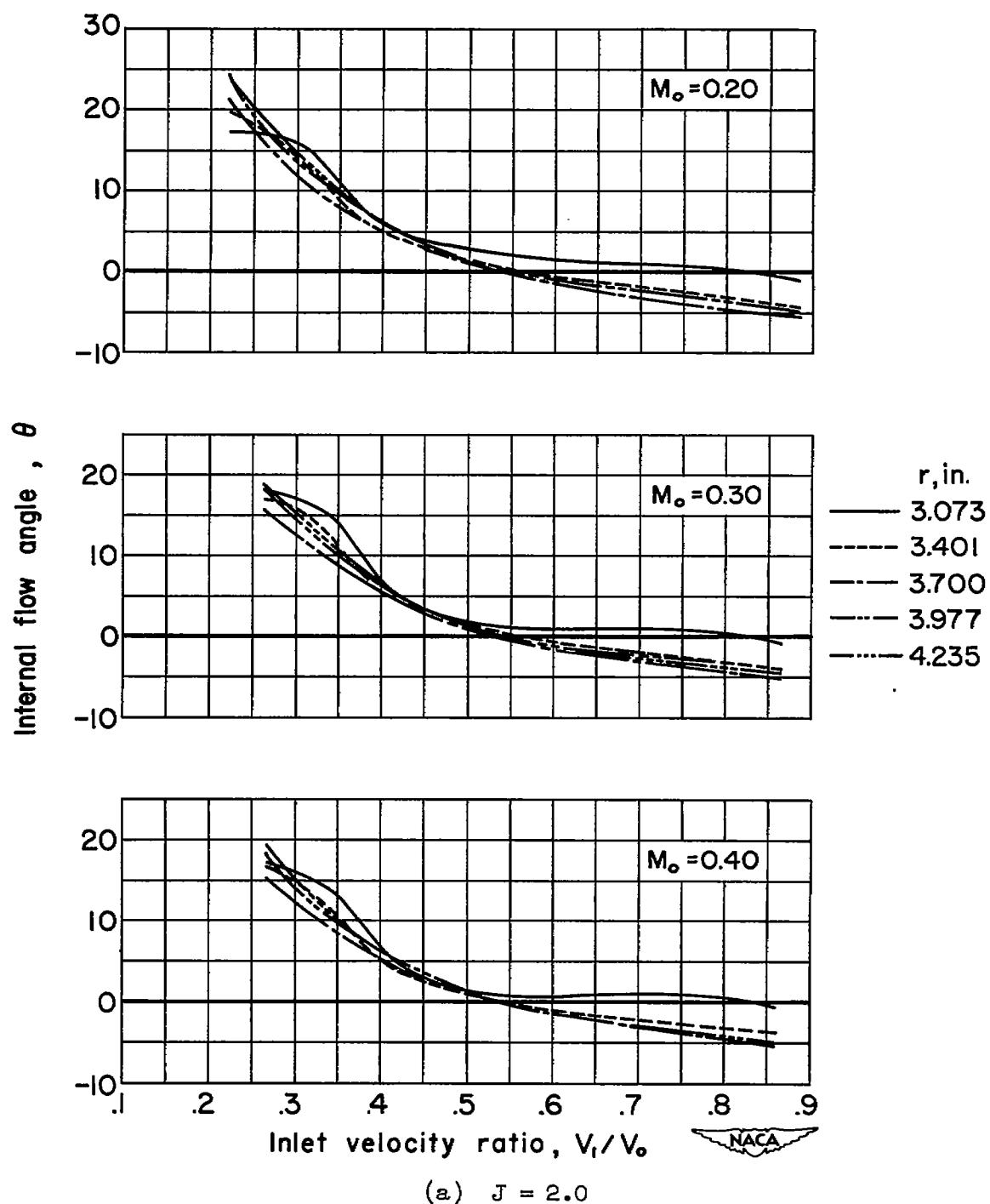
(a) J = 2.0

Figure 13.- The effect of inlet velocity ratio on the internal
flow angle.
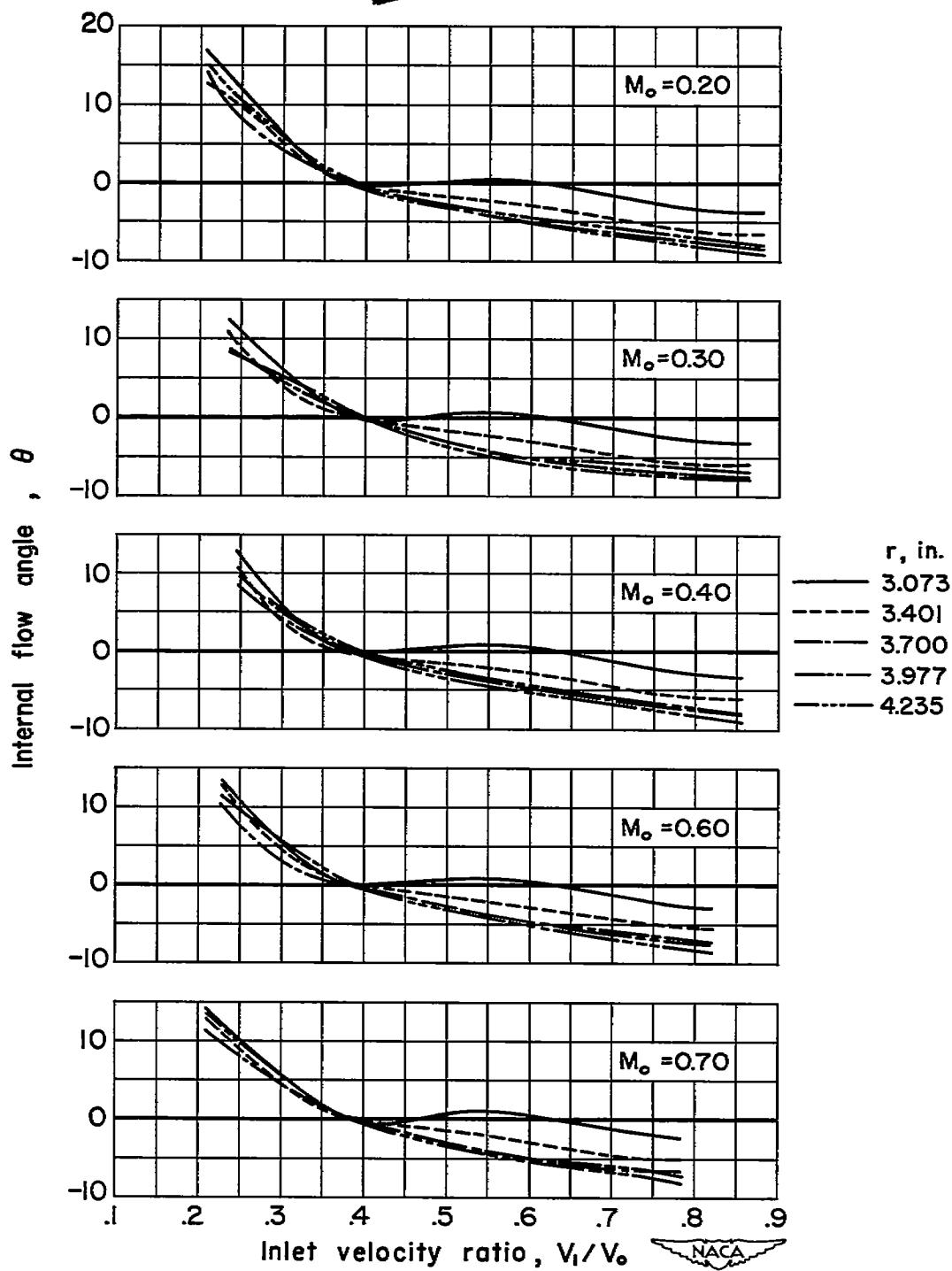
(b) J = 2.8

Figure 13.- Continued.

r, in.
——— 3.073
————— 3.401
—·—· 3.700
—··—·· 3.977
—···—··· 4.235
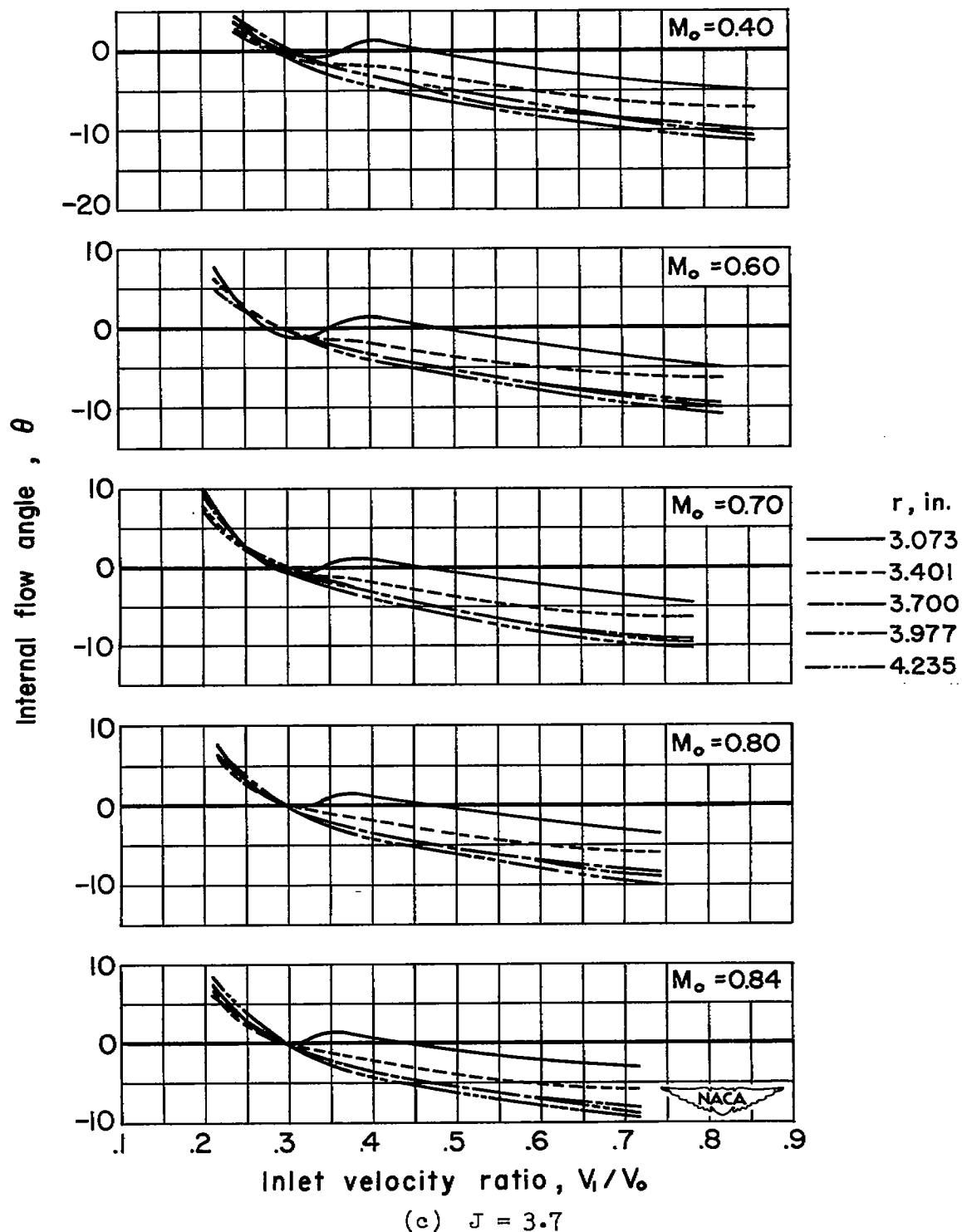
(c)   J = 3.7

Figure 13.- Concluded.
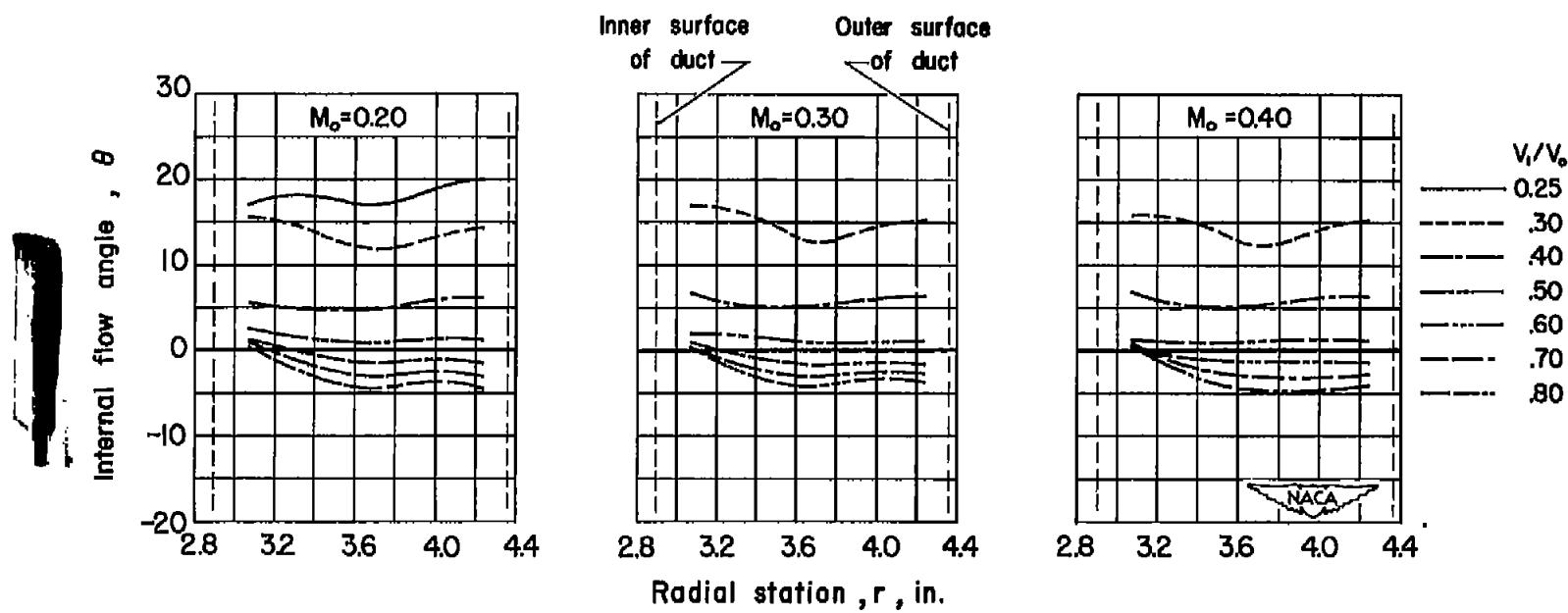
(a) J = 2.0

Figure 14.- The variation of the internal flow angle across the duct.
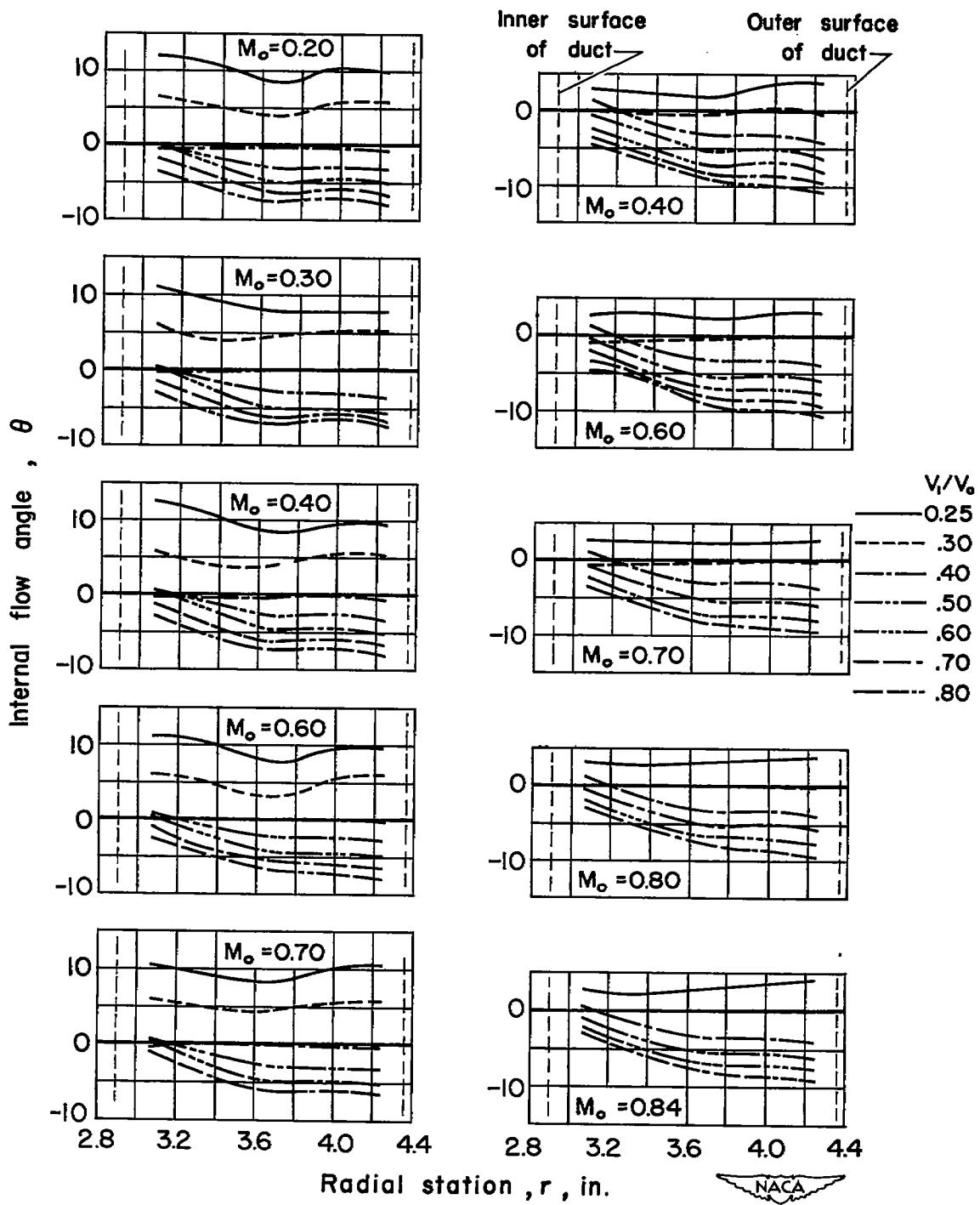
(b) J = 2.8

(c) J = 3.7

Figure 14.- Concluded.

V_1/V_o		V_1/V_o		V_1/V_o	
o	0.22	o	0.21	o	0.21
□	.32	□	.31	□	.26
◇	.42	◇	.39	◇	.35
△	.61	△	.53	△	.54
▽	.76	▽	.68	▽	.72
▷	.93	▷	.74		
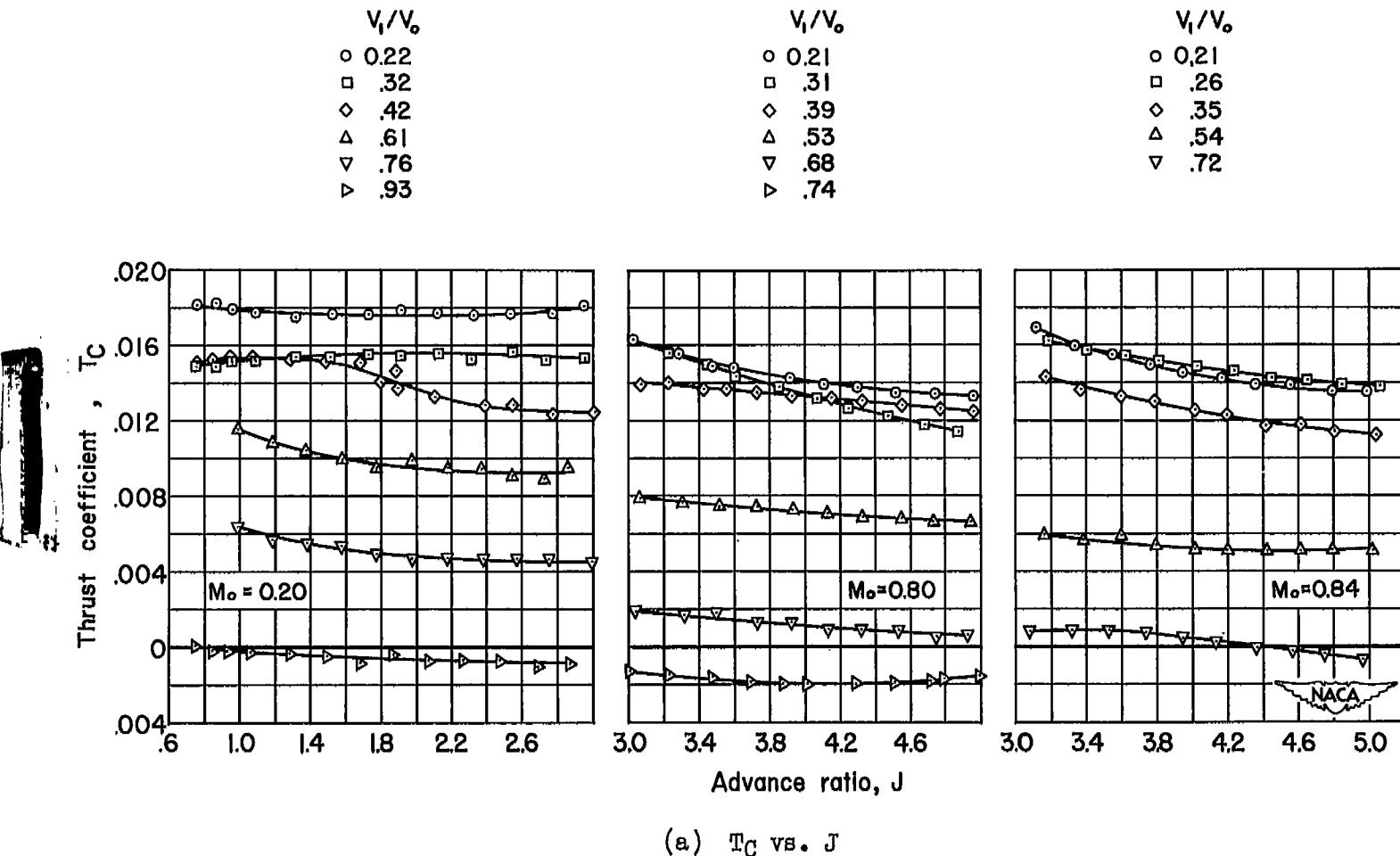
(a) T_C vs. J

Figure 15.- Typical force characteristics of the NACA 1-51-117 rotating E-cowl.
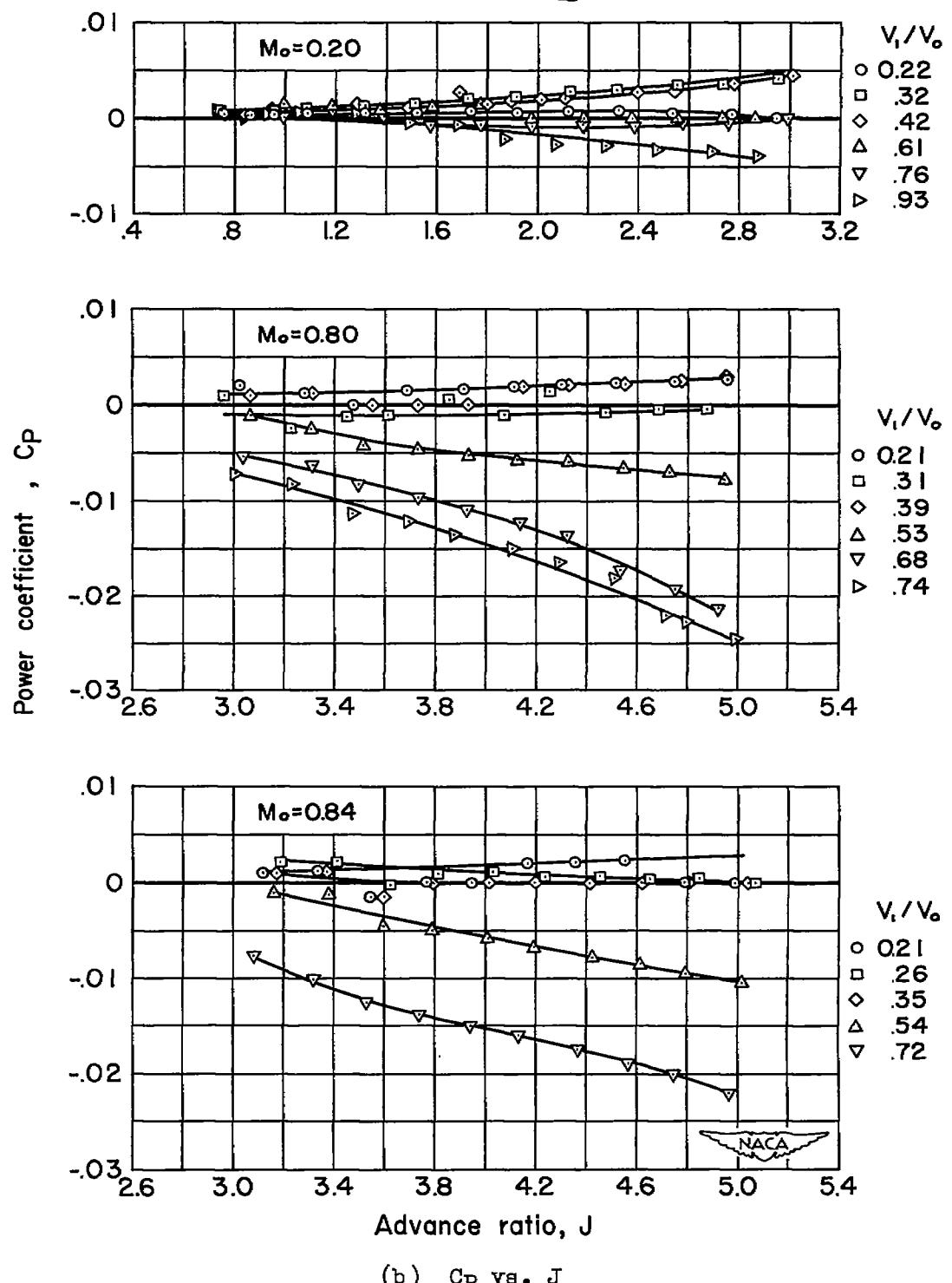
(b) C_P vs. J

Figure 15.- Continued.

(c) T_C vs. V_1/V_O
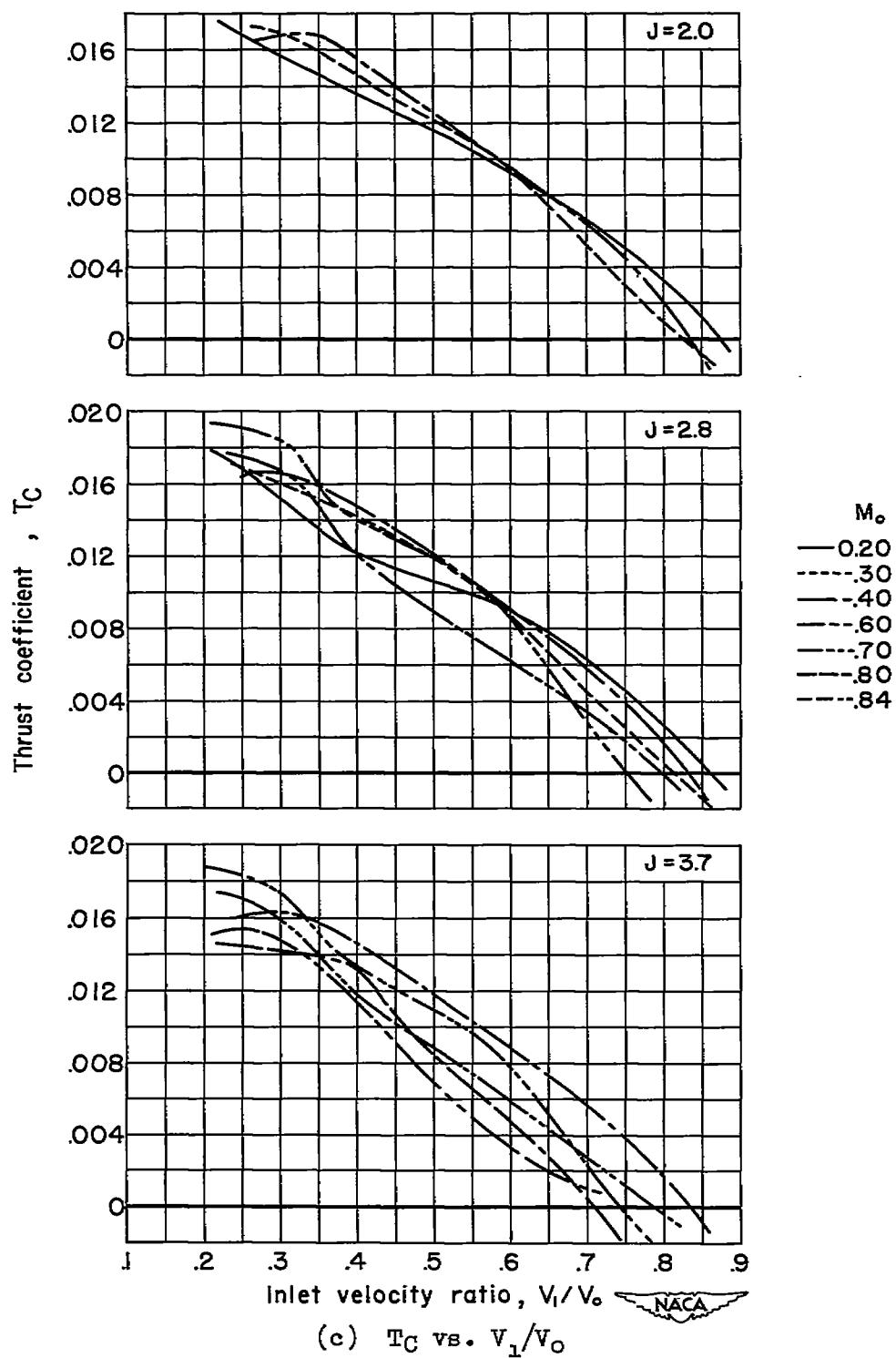
Figure 15.- Continued.
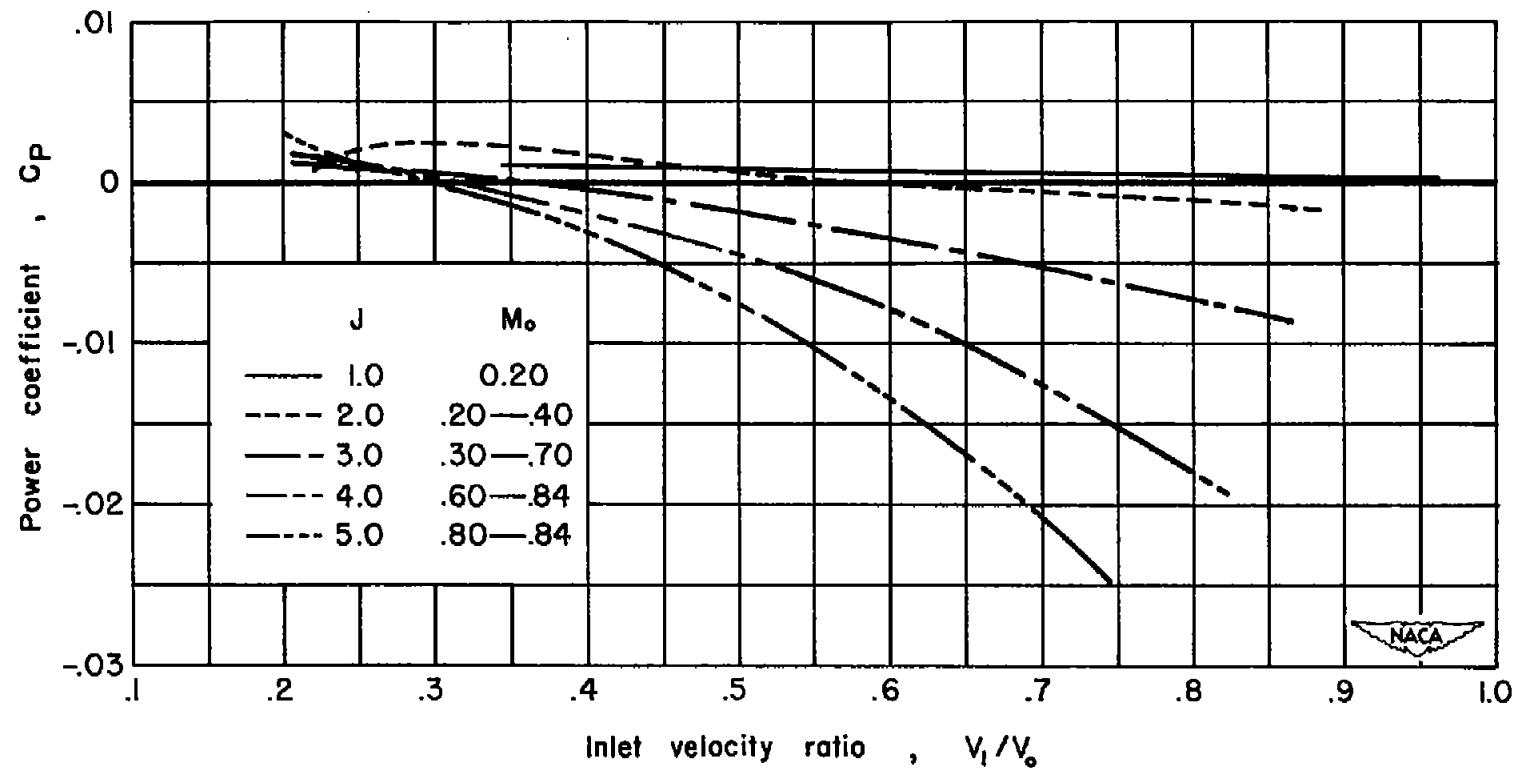
(d) C_P vs. V_1/V_0

Figure 15.- Concluded.

(a) $M_O = 0.20$

(b) $M_O = 0.84$
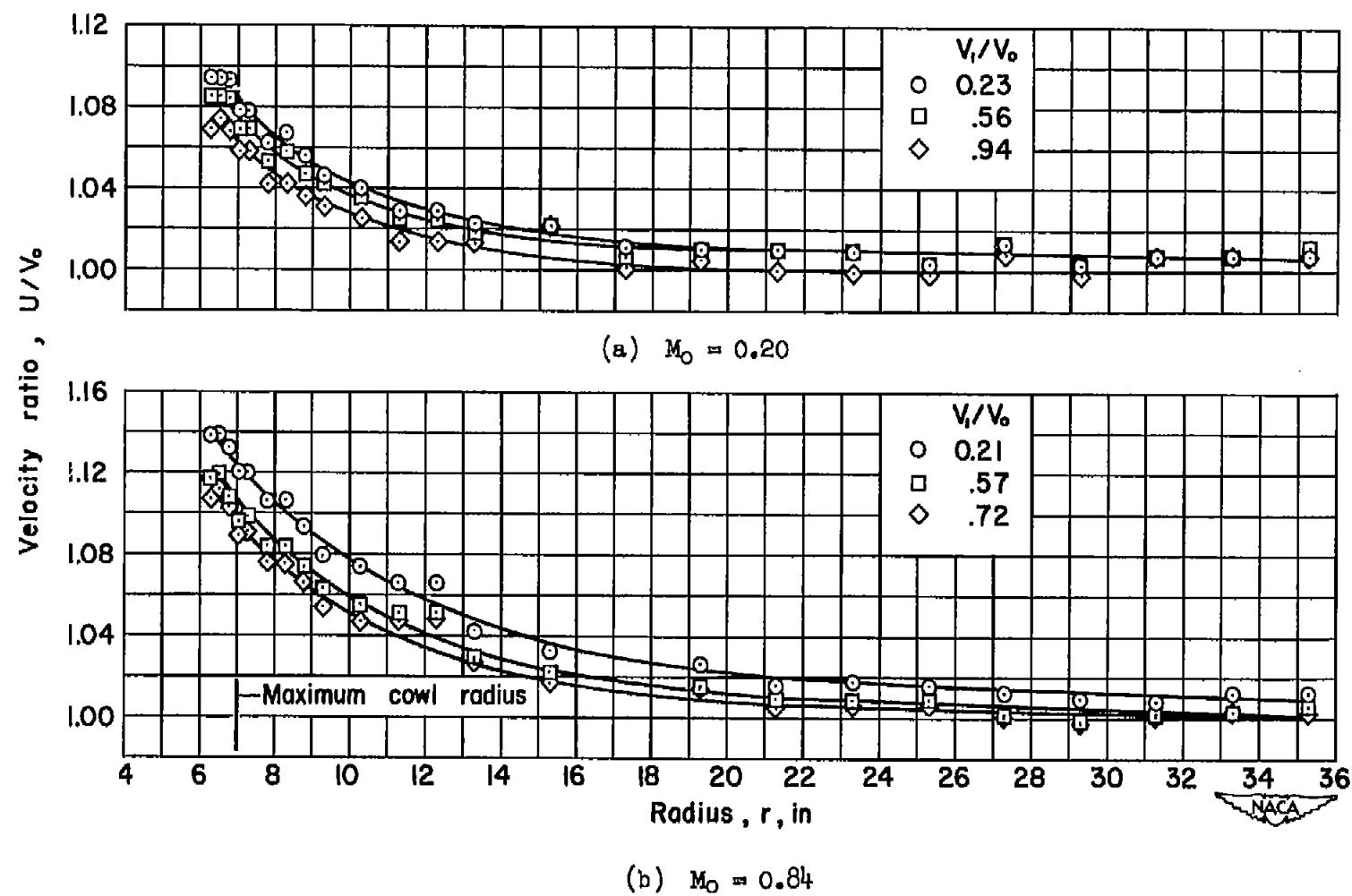
Figure 16.- Typical radial distributions of the local velocity ratio in the propeller plane.
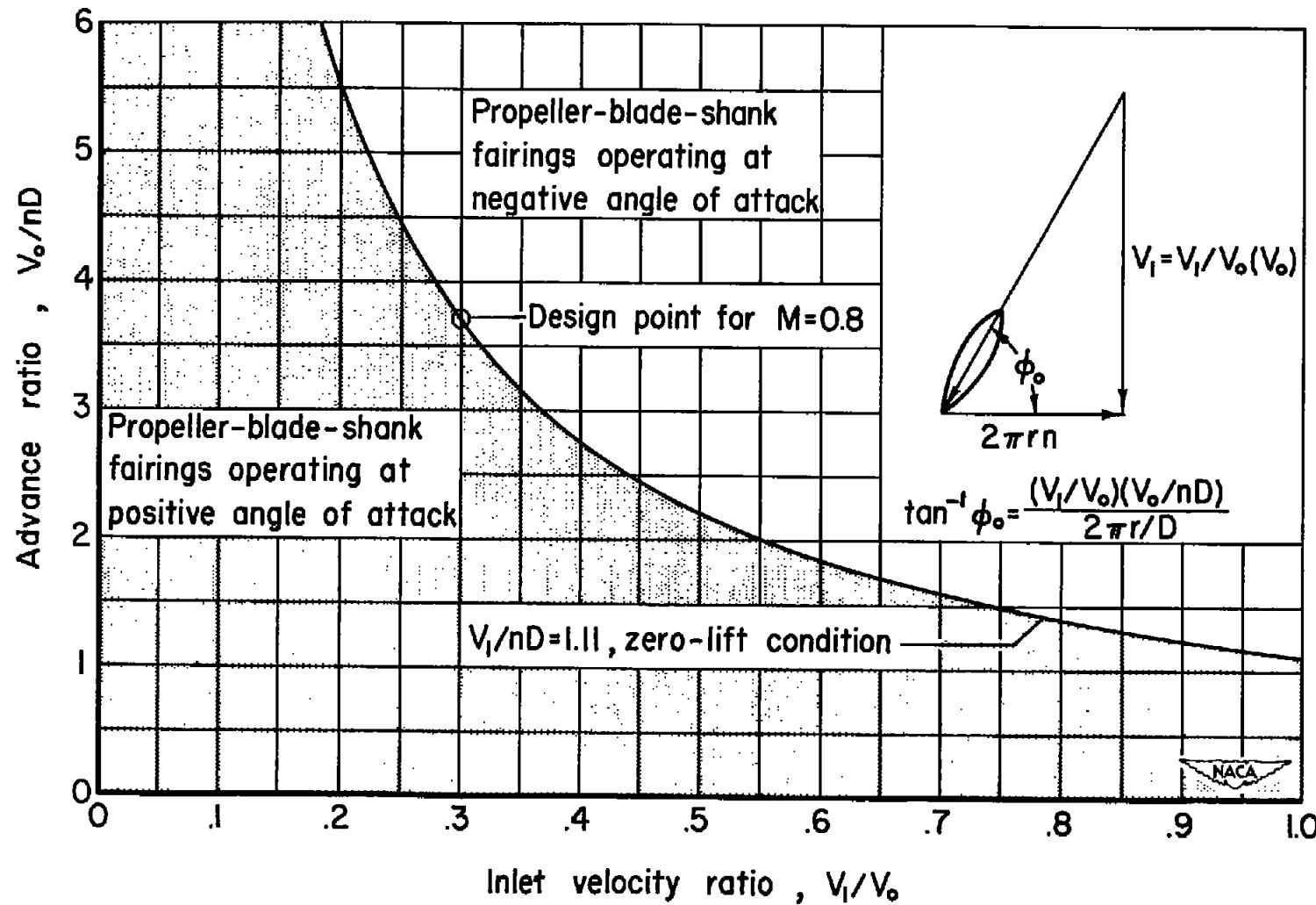
Figure 17.- The effect of inlet velocity ratio and advance ratio on the operating conditions for the propeller-blade-shank fairings.